Molecular Therapy
Original Article

CXCL11-armed oncolytic adenoviruses enhance CAR-T cell therapeutic efficacy and reprogram tumor microenvironment in glioblastoma

Guoqing Wang,[1,4] Zongliang Zhang,[2,4] Kunhong Zhong,[2] Zeng Wang,[2] Nian Yang,[2] Xin Tang,[1] Hexian Li,[2] Qizhong Lu,[2] Zhiguo Wu,[2] Boyang Yuan,[1] Meijun Zheng,[3] Ping Cheng,[2] Aiping Tong,[2] and Liangxue Zhou[1]

[1]Department of Neurosurgery, West China Hospital, West China Medical School, Sichuan University, Chengdu 610041, PR China; [2]State Key Laboratory of Biotherapy and Cancer Center, Research Unit of Gene and Immunotherapy, Chinese Academy of Medical Sciences, Collaborative Innovation Center for Biotherapy, West China Hospital, Sichuan University, Chengdu 610041, PR China; [3]Department of Otolaryngology, Head and Neck Surgery, West China Hospital, West China Medical School, Sichuan University, Chengdu 610041, PR China

Glioblastoma (GBM) is the most aggressive primary malignant brain cancer and urgently requires effective treatments. Chimeric antigen receptor T (CAR-T) cell therapy offers a potential treatment method, but it is often hindered by poor infiltration of CAR-T cells in tumors and highly immunosuppressive tumor microenvironment (TME). Here, we armed an oncolytic adenovirus (oAds) with a chemokine CXCL11 to increase the infiltration of CAR-T cells and reprogram the immunosuppressive TME, thus improving its therapeutic efficacy. In both immunodeficient and immunocompetent orthotopic GBM mice models, we showed that B7H3-targeted CAR-T cells alone failed to inhibit GBM growth but, when combined with the intratumoral administration of CXCL11-armed oAd, it achieved a durable antitumor response. Besides, oAd-CXCL11 had a potent antitumor effect and reprogramed the immunosuppressive TME in GL261 GBM models, in which increased infiltration of $CD8^+$ T lymphocytes, natural killer (NK) cells, and M1-polarized macrophages, while decreased proportions of myeloid-derived suppressor cells (MDSCs), regulatory T cells (Tregs) and M2-polarized macrophages were observed. Furthermore, the antitumor effect of the oAd-CXCL11 was $CD8^+$ T cell dependent. Our findings thus revealed that CXCL11-armed oAd can improve immune-virotherapy and can be a promising adjuvant of CAR-T therapy for GBM.

INTRODUCTION

Glioblastoma (GBM) is a highly aggressive and malignant primary brain tumor in adults and is intractably resistant to therapy.[1] Despite receiving the standard of care such as surgical resection, radiotherapy, and chemotherapy, only a 15-month median survival is observed.[2,3]

Chimeric antigen receptor T (CAR-T) cells have presented an amazing clinical antitumor effect in hematological malignancies, resulting in US Food and Drug Administration (FDA) approval of Kymriah, Yescarta, Tecartus, and Breyanzi and others for clinical use.[4] However, this success in hematological malignancies has not been repeated in solid tumors. The tumor microenvironment (TME) of malignant solid cancers is highly immunosuppressive, which provides multiple immune escape mechanisms. Insufficient tumor infiltration of CAR-T cells is also a key factor that impairs the translation of CAR-T therapy in solid cancers.[5,6]

Due to the unfavorable chemokine gradients within TME, the trafficking of CAR-T cells is always insufficient.[7] Several chemokines play an indispensable role in recruiting T cells, such as CXC ligand (CXCL) 9, 10, 11, 16, CCL5, CCL21, and CCL27.[8–11] The expression of these chemokines is highly correlated to T cell infiltration in tumors and significantly related to prolonged survival in cancer patients.[10,12–15]

Oncolytic viruses (OVs) provide a promising therapeutic approach for GBM, which can specifically infect, replicate, and lyse tumor cells while sparing normal cells.[16] Viral-mediated killing of tumor cells releases potent danger signals (pathogen-associated molecular patterns and damage-associated molecular patterns) as well as tumor-associated and -specific antigens that trigger both potent antitumor innate and adaptive immunity.[16–19] Apart from the selective tumor lysis and the activation of potential antitumor immunity, OVs can be genetically modified to express transgenes, which substantially enhances their antitumor efficacy, and have presented remarkable clinical

Received 25 April 2022; accepted 26 August 2022;
https://doi.org/10.1016/j.ymthe.2022.08.021.

[4]These authors contributed equally

Correspondence: Aiping Tong, PhD, State Key Laboratory of Biotherapy and Cancer Center, Research Unit of Gene and Immunotherapy, Chinese Academy of Medical Sciences, Collaborative Innovation Center for Biotherapy, West China Hospital, Sichuan University, Chengdu 610041, PR China.
E-mail: aipingtong@scu.edu.cn
Correspondence: Liangxue Zhou, MD, PhD, Department of Neurosurgery, West China Hospital, West China Medical School, Sichuan University, Chengdu 610041, PR China.
E-mail: liangxue_zhou@126.com

This is an open access article under the CC BY-NC-ND license (http://creativecommons.org/licenses/by-nc-nd/4.0/).

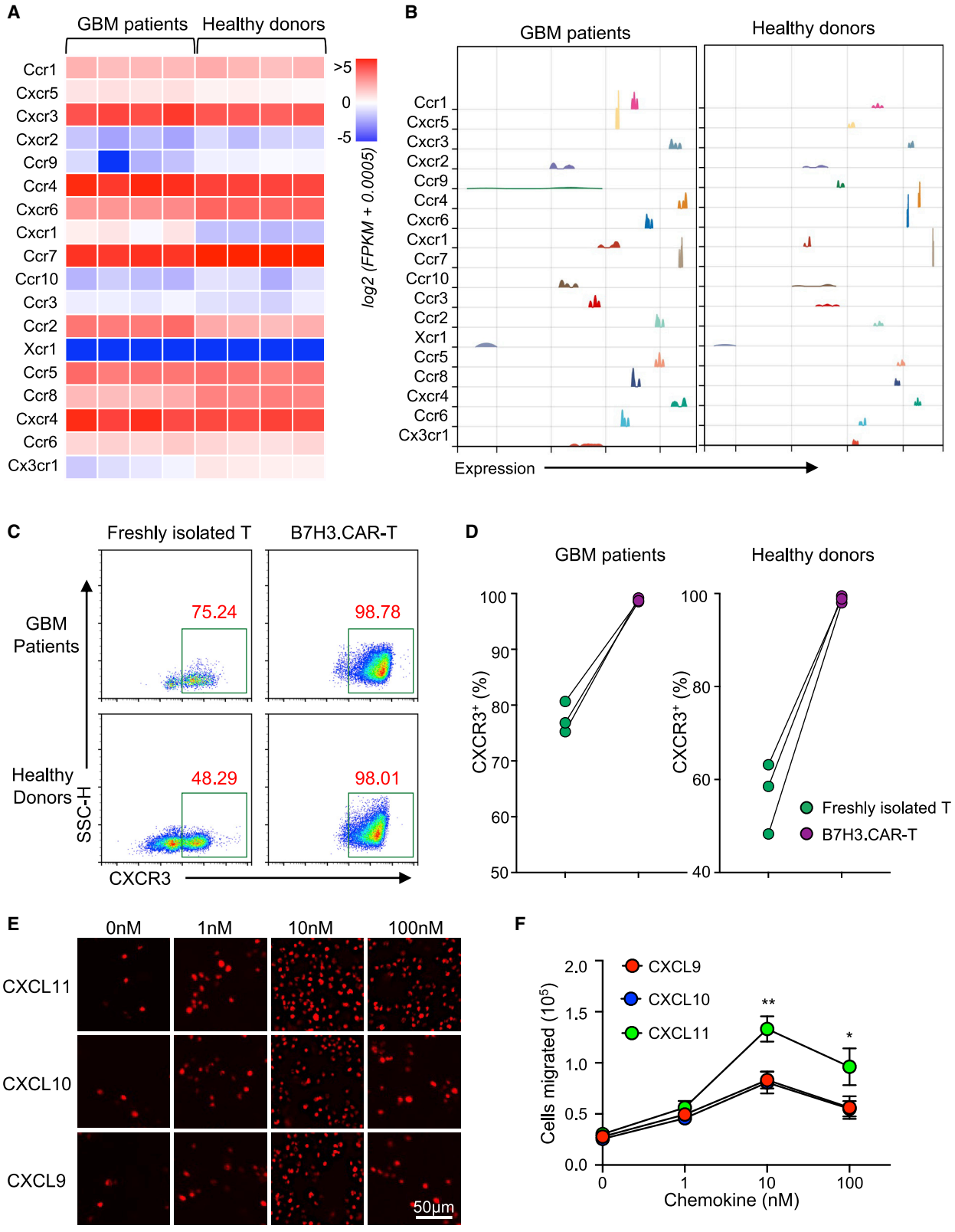

(legend on next page)

benefits in patients suffering solid tumors.[20,21] To solve the poor CAR-T cell infiltration in GBM, we exploited OVs to express a chemokine.

We thus engineered an oncolytic adenovirus with CXCL11 to improve subsequent recruitment of CAR-T cells and at the same time reprogram the immunosuppressive TME. In a xenograft GBM mice model, we showed that CXCL11-armed oncolytic adenovirus treatment increased the infiltration of CAR-T cells, and this combination strategy resulted in the effective control of established GBM. In a syngeneic GBM mice model, we showed that CXCL11-armed oncolytic adenovirus treatment resulted in a potent antitumor effect against established gliomas and reprogramed the TME of GBM. Our results showed that CXCL11-armed oncolytic adenovirus may improve the infiltration of CAR-T cells into the TME, reprogram immunosuppressive TME of GBM, and thus offer a potential approach for a combinatorial therapeutic strategy in clinical studies.

RESULTS

T cells express high levels of CXCR3, and CXCL11 is an ideal ligand to attract CAR-T cells

In order to analyze the chemokine receptors expressed on T cells, human T cells were freshly collected from peripheral blood mononuclear cells (PBMCs) of four GBM patients and four healthy donors, and then RNA sequencing (RNA-seq) analysis was conducted. The expression level of chemokine receptors was displayed by a heatmap (Figure 1A) and a ridgeline plot (Figure 1B). CXCR3 was a strongly expressed chemokine receptor on T cells of both GBM patients and healthy donors. We further analyzed chemokine receptors expressed on murine T cells based on the RNA-seq data from the GEO database (dataset: GSE187545). CXCR3 was also strongly expressed on murine T cells, especially memory T cells (Figure S1). In order to compare the change of CXCR3 expression between T and CAR-T cells, we first analyzed the expression levels of CXCR3 on T cells freshly isolated from healthy donors and patients with GBM. Then, after their CAR-T cells were produced, CXCR3 expression on CAR-T cells was analyzed again. Freshly isolated T cells highly expressed CXCR3, and CAR-T cells further increased the CXCR3 expression (Figures 1C and 1D). Then, we attempted to find an ideal chemokine to attract them. Transwell assay was used to assess the chemotactic ability of three chemokine ligands of CXCR3 (CXCL9, CXCL10, and CXCL11) to CAR-T cells. The results indicated that CXCL11 is more potent than CXCL9 or CXCL10 as a chemoattractant to CAR-T cells (Figures 1E and 1F).

Construction and characterization of the CXCL11-armed oncolytic adenoviruses

We constructed new oncolytic adenoviruses (oAds) expressing human CXCL11 or not based on human adenovirus 5 (Ad5). These OVs contained the delta E3-reserved adenovirus death protein (ADP) structure. Most E3 genes of the virus were deleted except for the ADP, which can facilitate oncolytic efficacy and viral spread. E1A gene was controlled by an hTERT promoter. These oncolytic adenoviruses are termed as oAd and oAd-CXCL11. The genetic maps of oAd and oAd-CXCL11 with EGFP insertion or not are illustrated (Figures 2A and S2A). To demonstrate whether oAd-CXCL11 causes no toxicity to CAR-T cells, we first detected the expression level of the Coxsackie-adenovirus receptor (CXADR) in five GBM cell lines, GBM patient-derived GBM23 and B7H3.CAR-T cells. In Figure 2B, flow cytometry shows that all GBM cell lines and GBM23 cells expressed the CXADR, whereas B7H3.CAR-T cells did not. Next, the replication functionality of this genetically engineered adenovirus with its parental virus in GBM cells was detected. We infected U87, U251, and GBM23 cells with oAd-CXCL11 or parental virus oAd (multiplicity of infection [MOI] = 0.1 or 1) and then measured the replication efficiency over time using $TCID_{50}$ assays. The two OVs presented similar replication capability in GBM cells (Figures 2C and S3). The virus replication was also confirmed by the expression of E1A protein at different times post infection in U87 cells (Figure 2D). To verify the expression of the chemokine CXCL11, U87 cells were infected with oAd or oAd-CXCL11 at an MOI of 1, or mock infected. After 48 h post infection, conditioned media were harvested. The production of CXCL11 protein was measured using ELISA assay. U87 cells infected with oAd-CXCL11 secreted more CXCL11 in the supernatant compared with uninfected or oAd groups (Figure 2E). In addition, the expression of CXCL11 was accumulated as the oAd-CXCL11 replicated in U87 cells (Figure 2D). Coculture with the oAd or oAd-CXCL11 induced similar cytotoxicity in U87, U251, and GBM23 cells in a dose-dependent fashion (Figure 2F), but B7H3.CAR-T cells were not affected (Figure S4). To assess the tumor cells' apoptosis after they were infected with oAd or oAd-CXCL11, we collected the GBM cells 24 h post infection and stained them with Annexin V/7-AAD. Tumor cell early apoptosis was efficiently induced by both oAd and oAd-CXCL11, compared with the uninfected tumor cells (Figures 2H and 2I). In addition, the expression of cleaved Caspase-3 was accumulated as the oAd-CXCL11 replicated in the U87 cells (Figure 2G). Taken together, these results demonstrated that the chemokine CXCL11 was secreted from oAd-CXCL11-infected cells *in vitro* and the CXCL11 gene insertion did not impair the replicating and oncolytic efficacy of the virus.

Figure 1. CXCR3 is highly expressed on freshly isolated T cells and CXCL11 was a potent ligand to attract CAR-T cells

(A and B) Heatmap (A) and ridgeline plot (B) of expression of chemokine receptor genes in the human T cells (both GBM patients and healthy donors). (C) The expression of CXCR3 on freshly isolated T cells from GBM patients and healthy donors and their corresponding B7H3.CAR-T cells were measured by flow cytometry. (D) Summary data of (C). (E) Media were supplemented with various concentrations of recombinant CXCL9, CXCL10, and CXCL11, after which Transwell assay was performed and the directional movements of B7H3.CAR-T cells were monitored. (F) Summary data of (E). Scale bar, 50 μm. The statistical analysis was estimated by one-way ANOVA with Tukey's correction. Data are presented as mean values ±SD. *$p < 0.05$, **$p < 0.01$.

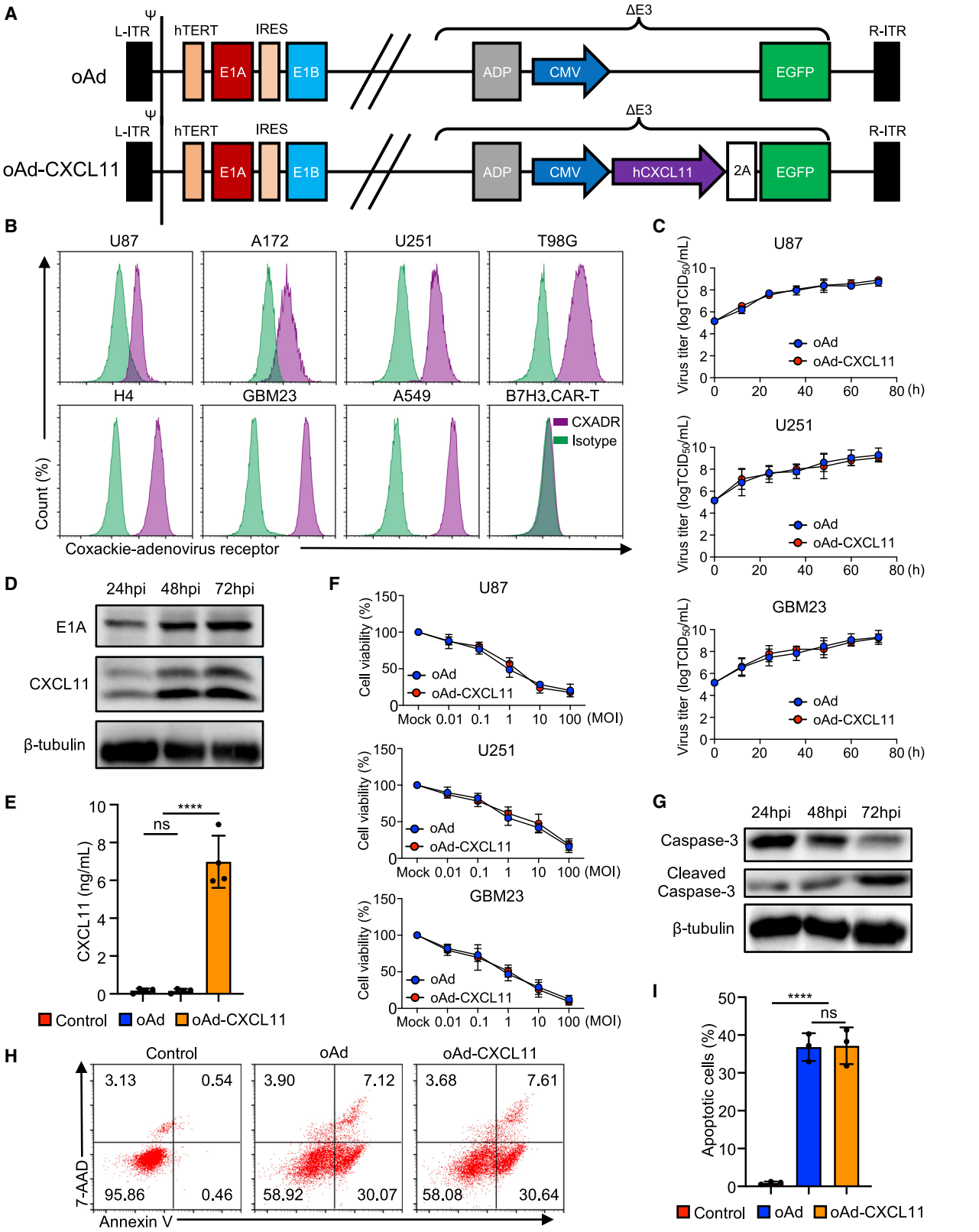

(legend on next page)

Construction of B7H3.CAR-T cells and oAd-CXCL11 enhances the migration and infiltration of B7H3.CAR-T cells

After confirming B7H3 expression on GBM cell lines as well as GBM patient-derived GBM23 cells (Figure 3A), whereas there was low expression on normal tissues or cells based on online databases (Figure S5), we generated B7H3-targeted second-generation CAR with 4-1BB costimulatory domain, inserted with mCherry or not and a control CAR targeting CD19 (Figures 3B and S2B). The CAR expression on T cells was assessed through analyzing the co-expressed fluorescence marker mCherry (Figure S6A) and flow cytometry (Figure S6B), respectively. The cytotoxic ability of B7H3.CAR-T cells was confirmed in U87, U251, and GBM23 cells (Figure S7). *In vitro* migration assays confirmed that GBM cells infected with oAd-CXCL11 other than the parental oAd improved the migration of B7H3.CAR-T cells (Figures 3C–3E). Next, *in vitro* infiltration assays confirmed that 3D tumor spheroids of U87-mCherry cells infected with oAd-CXCL11, rather than oAd, increased the infiltration of B7H3.CAR-T cells (Figures 3F–3H). In summary, these results suggested that oAd-CXCL11 increased the migration and infiltration of B7H3.CAR-T cells *in vitro*.

Combined oAd-CXCL11 and B7H3.CAR-T cells have a better cytotoxic activity to GBM cells *in vitro*

To explore the antitumor efficacy of the combination of B7H3.CAR-T cells and oAd-CXCL11 *in vitro*, we performed a modified coculture assay based on Transwell assay. U87 cells were infected with oAd, oAd-CXCL11, or saline control for 48 h. Then B7H3.CAR-T or CD19.CAR-T cells were added into upper chambers. Then, 24 h later, crystal violet staining assay showed superior cytotoxicity for combined oAd-CXCL11 and B7H3.CAR-T cells compared with combined oAd and B7H3.CAR-T cells (Figures 4A and 4B). We also performed a 2D coculture assay to evaluate the antitumor efficacy of monotherapy or combinatorial therapy by the xCELLigence real-time cell analysis (RTCA) system. Combination of B7H3.CAR-T cells and oAd-CXCL11 induced superior tumor cell killing activity (Figure 4C). Similarly, a 3D coculture assay using Calcein/PI staining also indicated that combined oAd-CXCL11 and B7H3.CAR-T cells induced superior cytotoxicity (Figure 4D) and higher levels of tumor necrosis factor alpha (TNF-α) as well as interferon gamma (IFN-γ) in culture media (Figure 4E).

oAd-CXCL11 enhances the antitumor effect of B7H3.CAR-T in an immunodeficient GBM mice model and increases tumor infiltration of CAR-T cells

To analyze the antitumor effect of combinatorial treatment of oAd-CXCL11 plus B7H3.CAR-T against GBM *in vivo*, we established an orthotopic patient-derived GBM mice model by intracranially delivering 1×10^5 luciferases (Luc)-expressing patient-derived GBM cells (GBM23-Luc) into NCG mice. Seven days post GBM cell infusion, mice were treated with an intratumoral administration with oAd, oAd-CXCL11 (5×10^8 plaque-forming units [PFU] per mouse), or saline as control. Then, 2 days later, mice were treated with an intravenous delivery with 5×10^6 B7H3.CAR-T. The bioluminescence signal of tumors was detected to reflect the growth of tumors (Figure 5A). Mice treated with saline control were observed to have rapid progression of tumor and were dead within 30 days, while the single administration of oAd-CXCL11 or B7H3.CAR-T both inhibited GBM progression moderately and prolonged the survival compared with saline control (Figures 5B–5D). Combination treatment of oAd-CXCL11 plus B7H3.CAR-T was significantly more effective than single treatment and combination treatment of oAd plus B7H3.CAR-T at controlling the growth of GBM tumors and improving the survival time *in vivo* (Figures 5B–5D). Four of five mice of the combination group survived over 70 days by the end of the study and showed nearly no detectable luciferase signal (Figure 5D). As the study progressed, the mice treated with oAd-CXCL11 plus B7H3.CAR-T gained steadily increasing body weights compared with the other groups (Figure 5E). At 25 days, H&E staining of representative slices from B7H3.CAR-T-treated mice showed large, space-occupying tumors; by comparison, mice that received oAd plus B7H3.CAR-T exhibited moderate repression, and mice that received oAd-CXCL11 and B7H3.CAR-T were dramatically smaller (Figure 5F). Furthermore, oAd-CXCL11 treatment induced substantially more accumulation of B7H3.CAR-T cells in tumors than B7H3.CAR-T monotherapy or combined oAd plus B7H3.CAR-T treatment based on immunostaining for CD3 (Figures 5F and 5G). Adenovirus protein was detected by immunostaining for E1A in oAd- or oAd-CXCL11-treated mice (Figure 5F). Quantification of CXCL11 in the tumor biopsies confirmed that this chemokine was produced only in mice inoculated with oAd-CXCL11 (Figure 5H). Moreover, consistent with the tumor infiltration of CAR-T cells, in mice that received the combination treatment

Figure 2. Construction and characterization of oAd and oAd-CXCL11

(A) Schema of oncolytic adenoviruses. Top: genetic map of control oncolytic adenovirus, oAd, with deletion of E3 region sparing adenovirus death protein (ADP), insertion of the hTERT promoter into the E1 region, and insertion of EGFP gene into the E3 region. Bottom: genetic map of oAd-CXCL11 showing the inserted coding gene of the human CXCL11. (B) GBM cell lines and B7H3.CAR-T cells were explored for the expression levels of coxsackie-adenovirus receptor (CXADR) by flow cytometric analysis. A549, a lung carcinoma cell line, was utilized as a positive control. Green and purple filled lines correspond to isotype control and CXADR, respectively. (C) Human U87 glioma cells, U251 glioma cells, and GBM patient-derived GBM23 cells were challenged with oAd and oAd-CXCL11 at an MOI of 1. The oncolytic adenovirus titers were measured using $TCID_{50}$ assay at different time points post infection. (D) The replication of the oncolytic virus and secretion of CXCL11 at different times post infection were confirmed by immunoblot. (E) The quantity of secreted CXCL11 was measured in the culture media harvested from infected GBM cells by ELISA assay. (F) U87, U251 glioma cells, and GBM patient-derived GBM23 cells were infected with different titers of oAd-CXCL11 or with the control adenovirus oAd and measured 48 h later by MTT assay. (G) Cell lysate of oAd-CXCL11-infected U87 cells was harvested. Full-length Caspase-3 and cleaved Caspase-3 were detected by immunoblot. (H) U87 glioma cells were infected with saline control, oAd, or oAd-CXCL11 at an MOI of 1 for 24 h. The early apoptotic cells were confirmed as the 7-AAD$^-$/Annexin V$^+$ population. (I) Summary data of (H). All data were presented in at least three independent experiments. The statistical analysis was estimated by one-way ANOVA with Tukey's correction. Data are presented as mean values ±SD. ****$p < 0.0001$; ns, not significant.

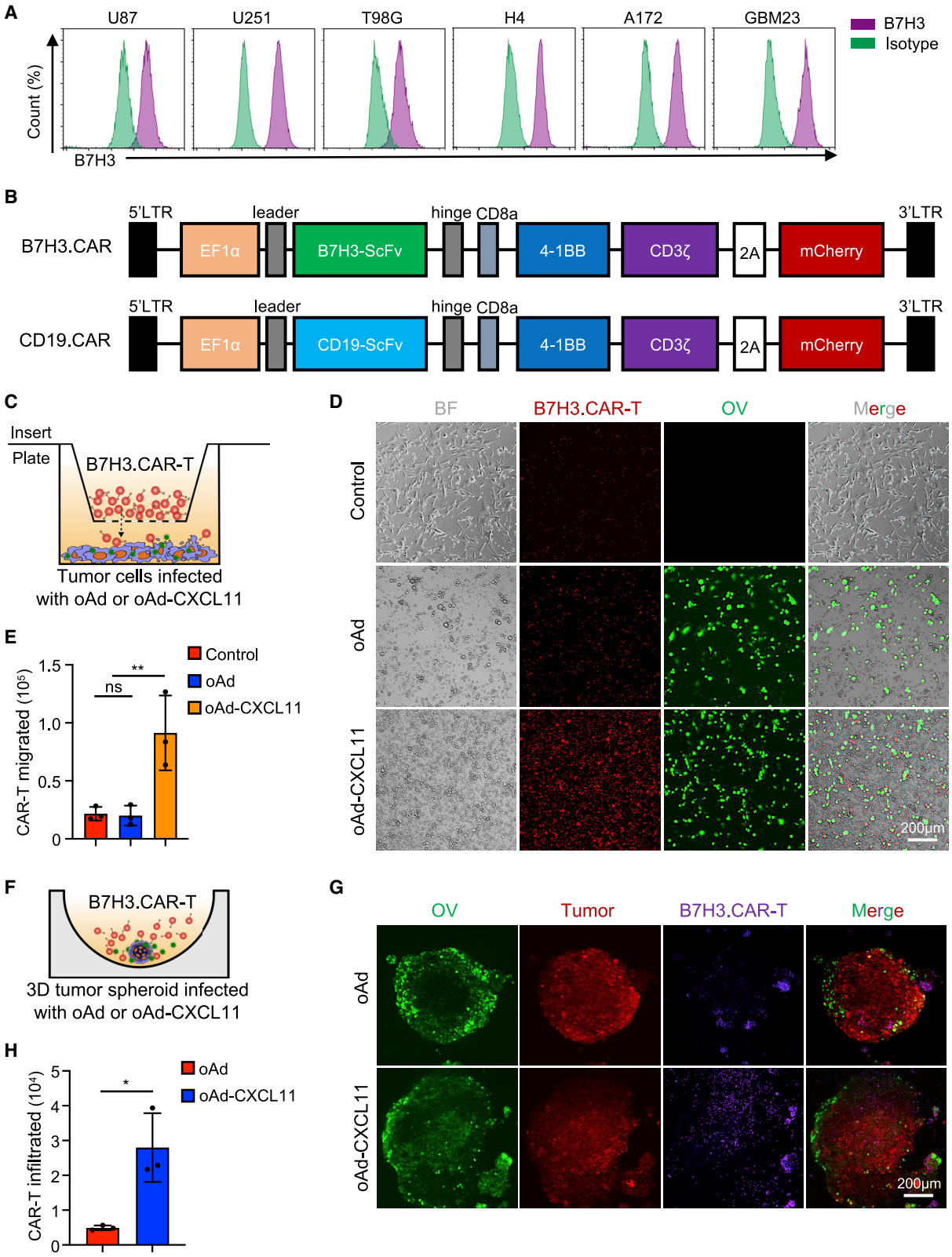

(legend on next page)

of oAd-CXCL11 plus B7H3.CAR-T, higher production of inflammatory cytokines (TNF-α, IFN-γ) was measured (Figures 5I and 5J). These data indicate that tumor treatment with either oAd-CXCL11 or B7H3.CAR-T only yielded limited therapeutic benefits, and only their combined use resulted in long-term and thorough antitumor effects.

oAd-CXCL11 is superior to oAd in producing a better outcome in a fully immunocompetent GBM model

Considering the deficiency of immune TME in NCG mice, in order to explore the effect of oAd-CXCL11 on TME, an immunocompetent GBM mice model was used to test the effectiveness of oAd-CXCL11. First, we modified the oAd and oAd-CXCL11 mentioned above by replacing the human CXCL11 gene with murine CXCL11 gene for the GL261 mice model (Figure 6A). In this study, a GL261 mouse GBM model susceptible to oAd infection was utilized (Figure S8). By intracranial injection of 1×10^5 GL261 cells into immunocompetent wild-type C57BL/6 mice, with slight modifications, we repeated the survival study in Figure 5 in an immunocompetent mouse model of GBM (Figure 6B). We set up three different treatment groups: saline, oAd, and oAd-CXCL11. Three days after GL261 cell infusion, mice were treated with an intratumoral administration with oAd or oAd-CXCL11 (5×10^8 PFU per mouse), or saline as control. The bioluminescence signal of tumors was detected to reflect the growth of tumors (Figure 6B). oAd in the immunocompetent mouse model had a similar moderate antitumor efficacy to oAd-CXCL11 in the immunodeficient mouse model. oAd moderately controlled tumor progression and prolonged survival compared with saline control (Figures 6C–6E). The mice treated with oAd-CXCL11 significantly slowed the progression of GBM and prolonged the survival compared with oAd- or saline control-treated mice (Figures 6C–6E). As the study progressed, the mice treated with oAd-CXCL11 gained steadily increasing body weights compared with the other groups (Figure 6F).

oAd-CXCL11 reprograms the TME toward a more beneficial state for antitumor immunity

We hypothesized that oAd-CXCL11-mediated alteration of immune TME might underlie the efficacy of its monotherapy. Therefore, tumor tissues were harvested 12 days after treatment, and the infiltrated immune cells within the TME were analyzed by flow cytometry. The flow cytometry gating strategy of this experiment is shown in Figure S9. A significant increase of infiltrating $CD45^+$ lymphocytes (Figure S10), and $CD3^+$ and $CD8^+$ T lymphocytes, but not $CD4^+$ T lymphocytes, was detected in oAd-CXCL11-treated GL261 tumors compared with oAd and saline control groups (Figures 7A, 7B, and 7G–7I). oAd also improved the infiltration of natural killer (NK) cells compared with saline control, which was further increased by oAd-CXCL11 (Figures 7C and 7J). Similarly, oAd reprogramed M2-like macrophages to a more proinflammatory M1-like phenotype within the TME compared with saline control, which was further improved by oAd-CXCL11 (Figures 7D, 7K, and 7L). In contrast, oAd-CXCL11 caused a remarkable loss of myeloid-derived suppressor cells (MDSCs) and regulator T cells (Tregs) compared with both oAd and saline control groups (Figures 7E, 7F, 7M, and 7N). These results suggest that oAd-CXCL11 reprogramed the immunosuppressive TME toward a more immunostimulatory condition.

The antitumor effect of oAd-CXCL11 is mediated by $CD8^+$ T cells

Considering the recruitment of NK cells and $CD8^+$ T cells induced by oAd-CXCL11, to confirm their critical role after virus administration, we depleted $CD8^+$ T or NK cells in GL261-bearing mice by anti-CD8a or anti-NK1.1 antibodies, respectively (Figure 8A). The flow cytometry showed that most $CD8^+$ T cells or NK cells in the peripheral blood were depleted in GBM-bearing mice 5 days after the last anti-CD8a or anti-NK1.1 antibody injection, respectively (Figure S11). In mice lacking $CD8^+$ T cells, the antitumor efficacy of oAd-CXCL11 was completely abrogated, but it was unaffected when using anti-NK1.1 antibodies (Figures 8B and 8C). In summary, these results revealed that the tumor-suppressing efficacy was mediated by $CD8^+$ T rather than NK cells.

oAd-CXCL11 facilitates the antitumor effect of B7H3.CAR-T in an immunocompetent GBM model and increases CAR-T cell infiltration

An immunocompetent GL261 GBM model was utilized to assess the antitumor effect of combinatorial treatment of oAd-CXCL11 plus B7H3-targeted murine CAR-T. Human B7H3 was transduced into the parental GL261 line. A second-generation CAR was designed including B7H3-specific ScFv, murine CD8-derived transmembrane region, murine 4-1BB, and CD3ζ intracellular regions. For confirmation of CAR-transduced T cells, a truncated mCD34 was co-expressed (Figure 8D). *In vivo*, $B7H3^+$ GL261 were efficiently killed by B7H3.CAR-T cells but not parental GL261 (Figure S12). Furthermore, we assessed the antitumor efficacy of murine CXCL11-armed oAd plus B7H3.CAR-T in mice suffering $B7H3^+$ GL261 GBM. By intracranial administration of 1×10^5 $B7H3^+$ GL261 cells into immunocompetent wild-type C57BL/6 mice, with slight modifications, we repeated the survival study in Figure 5 in an immunocompetent mouse model of GBM. Five days after $B7H3^+$ GL261 cell infusion,

Figure 3. oAd-CXCL11 improved the migration and infiltration of B7H3.CAR-T cells

(A) B7H3 expression on GBM cell lines and GBM23 cells was detected by flow cytometry. (B) Schematic of B7H3.CAR and CD19.CAR construct. (C) Schema of the Transwell assay. B7H3.CAR-T cells (2×10^5) were plated to the upper chambers and the lower chambers contained U87 cells (5×10^4) infected with oAd, oAd-CXCL11, or saline control. (D) Representative images showing the migration of B7H3.CAR-T cells. Scale bar, 200 μm. (E) Summary data of (D). (F) Schema of the chemotaxis experiment assessing the infiltration of B7H3.CAR-T cells into 3D tumor spheroid. 3D tumor spheroids of U87-mCherry cells were infected with oAd or oAd-CXCL11 at an MOI of 1 for 24 h. Then B7H3.CAR-T cells (5×10^4) were added to the wells. (G) Representative images showing the infiltration of B7H3.CAR-T cell. Scale bar, 200 μm. (H) Summary data of (G). The statistical analysis was estimated by one-way ANOVA with Tukey's correction. Data are presented as mean values ±SD. *$p < 0.05$; **$p < 0.01$; ns, not significant.

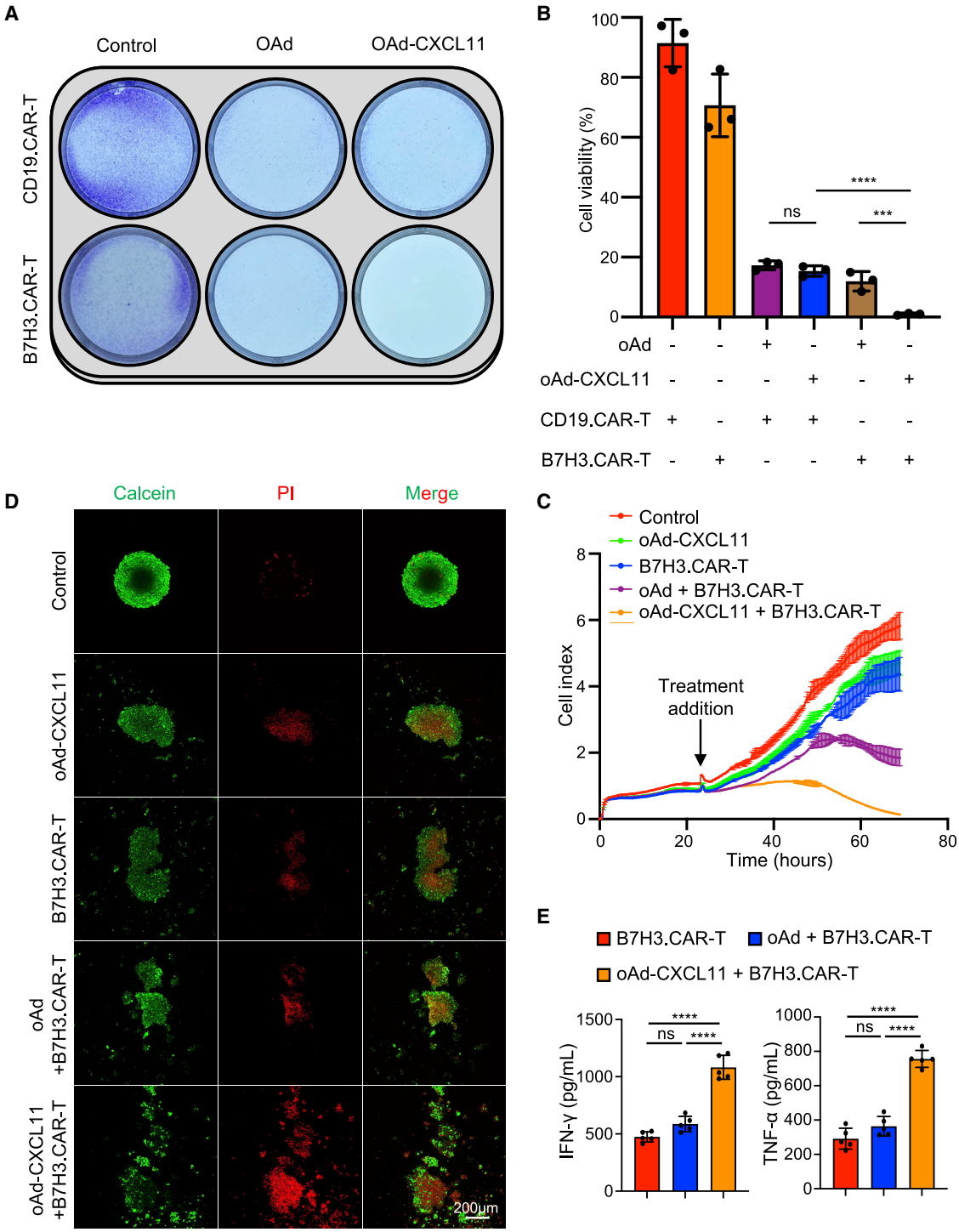

Figure 4. Combined oAd-CXCL11 and B7H3.CAR-T cells have a superior cytotoxic effect against GBM cells *in vitro*

(A) *In vitro* modified coculture assays based on Transwell experiments were used to assess the antitumor efficacy of either monotherapy or combination therapy. U87 cells were seeded and infected with oAd, oAd-CXCL11, or saline control for 48 h. Then B7H3.CAR-T or CD19.CAR-T cells were added to the upper chambers; 24 h later, cell viabilities were assessed using crystal violet staining assay, and (B) the viable and stained cells were counted. (C) The RTCA system was used to assess the antitumor effect of

(legend continued on next page)

mice were treated with an intratumoral administration with oAd or oAd-CXCL11 (5×10^8 PFU per mouse), or saline as control. Then, 2 days later, lymphodepletion was prepared by 5 Gy total body irradiation (TBI). Then, mice were treated with a single intravenous infusion of 5×10^6 CAR-T cells. The bioluminescence signal of GBM was detected to reflect the growth of tumors (Figure 8E). Combination treatment of oAd-CXCL11 plus B7H3.CAR-T was significantly more effective than B7H3.CAR-T single treatment and combination treatment of oAd plus B7H3.CAR-T at suppressing the growth of GBM tumors and prolonging their survival *in vivo* (Figures 8F–8H). Seven days after transfer, tumor-infiltrating CAR-T cells were shown by immunohistochemistry as well as flow cytometry for CD34 (Figure 8I). oAd-CXCL11 treatment induced substantially more CAR-T cell infiltration into tumor sites than CAR-T monotherapy or combined oAd plus CAR-T treatment (Figures 8J and 8K). In summary, these results demonstrated that CAR-T monotherapy failed to inhibit GL261 tumor and oAd-CXCL11 could facilitate the infiltration of CAR-T cells in tumors, thus eliciting a long-term and thorough antitumor effect.

DISCUSSION

In this study, oAd armed with CXCL11 increased the infiltration of CAR-T cells into GBM tumors and their combination contributed to superior inhibition of the tumor growth and prolonged survival of GBM-bearing NCG mice. We further adopted an immunocompetent GBM model to explore the antitumor effect of oAd-CXCL11 monotherapy and the modulation of TME induced by oAd-CXCL11. The results indicated that oAd-CXCL11 had a potent antitumor effect, which was mainly underpinned by oAd-CXCL11-elicited TME reprograming from a "cold" immunosuppressive to a "hot" immunosupportive state.

CAR-T therapy has achieved great success as a promising therapeutic approach to tumor treatment in hematological malignancies, but has only limited benefits for solid tumors due to several factors, including the immunosuppressive TME and the inadequate infiltration or trafficking of CAR-T cells.[6] In particular, GBM, an immunologically cold tumor, has extremely hostile conditions of the TME and insufficient infiltration of CAR-T cells.[22] Considering the two main challenges for CAR-T therapy against GBM, we have utilized a genetically modified oncolytic adenovirus carrying a chemokine, which is a "one-stone-kills-two-birds" strategy. On the one hand, oncolytic adenoviruses selectively infect and kill tumor cells *in situ* and reprogram the suppressive TME by reprograming the immune cells in the tumor sites.[23,24] On the other hand, adenoviruses have a large capacity of the genome and this long DNA sequence can be genetically modified to express transgenes.[20] Given this attractive feature, we incorporated the oncolytic adenovirus with a chemokine for recruiting CAR-T cells into GBM.

Trafficking of CAR-T cells into tumor sites relies upon the suitable expression of chemokine receptors on the CAR-T cells and their matched chemokines in the tumor sites.[25] To find the ideal chemokine receptor expressed on T cells, we conducted an RNA-seq analysis. RNA-seq of the chemokine receptors on T cells indicated that CCR4, CXCR4, CXCR3, and CCR7 were highly expressed on T cells. CCR4 is the receptor for CCL17 and CCL22 and is expressed especially on Treg cells.[26,27] Clinical data implicated that blockade of CCR4 was associated with increased intratumoral $CD8^+$ T cell infiltration.[28] CXCR4 is a chemokine receptor that is also overexpressed in most cancers and has important roles in tumor cell proliferation and dissemination as well as in angiogenesis.[29–31] CCR7 is expressed by B cells and by several subpopulations, including naive T cells[32,33] and Tregs.[34] Another highly expressed chemokine receptor, CXCR3, is highly expressed on effector or central memory T cells as well as CAR-T cells.[35,36] Given the above, CXCR3 was a highly expressed and more suitable candidate for exploitation to promote the trafficking of CAR-T cells.

Compared with freshly isolated T cells, nearly 100% of CAR-T cells expressed CXCR3, thus they were theoretically more inclined to be recruited by its ligands. This may be explained by the process of CAR-T cell production, in which CD3 and CD28 monoclonal antibodies (mAbs) were used to stimulate isolated T cells, and is consistent with the results that activated T and NK cells highly expressed CXCR3.[37] CXCR3, including both the splice variants, namely CXCR3-A and CXCR3-B, binds to the CXC subclass of chemokines, including CXCL9, CXCL10, CXCL11 (main CXCR3-A-ligand), and CXCL4 (main CXCR3-B-ligand).[38] CXCR3-A activation mediates proliferative and chemotactic responses. By comparison, CXCR3-B mediates anti-migratory and anti-proliferative effects.[39] Therefore, we mainly focused on the chemokines CXCL9, CXCL10, and CXCL11. These chemokines play crucial roles in the infiltration of CAR-T cells into TME.[40] However, there is a mismatch between chemokines and their corresponding receptors. A low amount of CXCR3 ligands exists within the tumor TME, which results in insufficient infiltration of $CXCR3^{high}$ $CD8^+$ T cells into tumors.[12] For instance, less than 1% of transferred CAR-T cells infiltrated flank tumors on the fifth day in an NCG xenograft model.[41] We performed a chemotaxis assay to explore which ligand possesses the most powerful chemotaxis to CAR-T cells. The results showed that, compared with CXCL9 or CXCL10, CXCL11 induced a significantly more potent chemotactic migration in CAR-T cells. In addition, the affinity of CXCL11 for CXCR3 has been demonstrated to be higher, with a more potent ability in stimulating calcium flux and receptor desensitization than CXCL9 or CXCL10.[42] These data indicated that CXCL11 is the dominant ligand for CXCR3. For optimized CAR-T cell trafficking, we therefore generated a genetically engineered oncolytic adenovirus, oAd-CXCL11, which infected GBM cells and

either monotherapy or combination therapy and the viable cells were calculated as the cell index. (D) Representative images showing the cytotoxic effect of either monotherapy or combined therapy against 3D spheroids of U87 cells by Calcein/PI staining. Scale bar, 200 μm. (E) Concentrations of TNFα and IFNγ in culture media were measured by ELISA. The statistical analysis was estimated by one-way ANOVA with Tukey's correction. Data are presented as mean values ± SD. ***$p < 0.001$; ****$p < 0.0001$; ns, not significant.

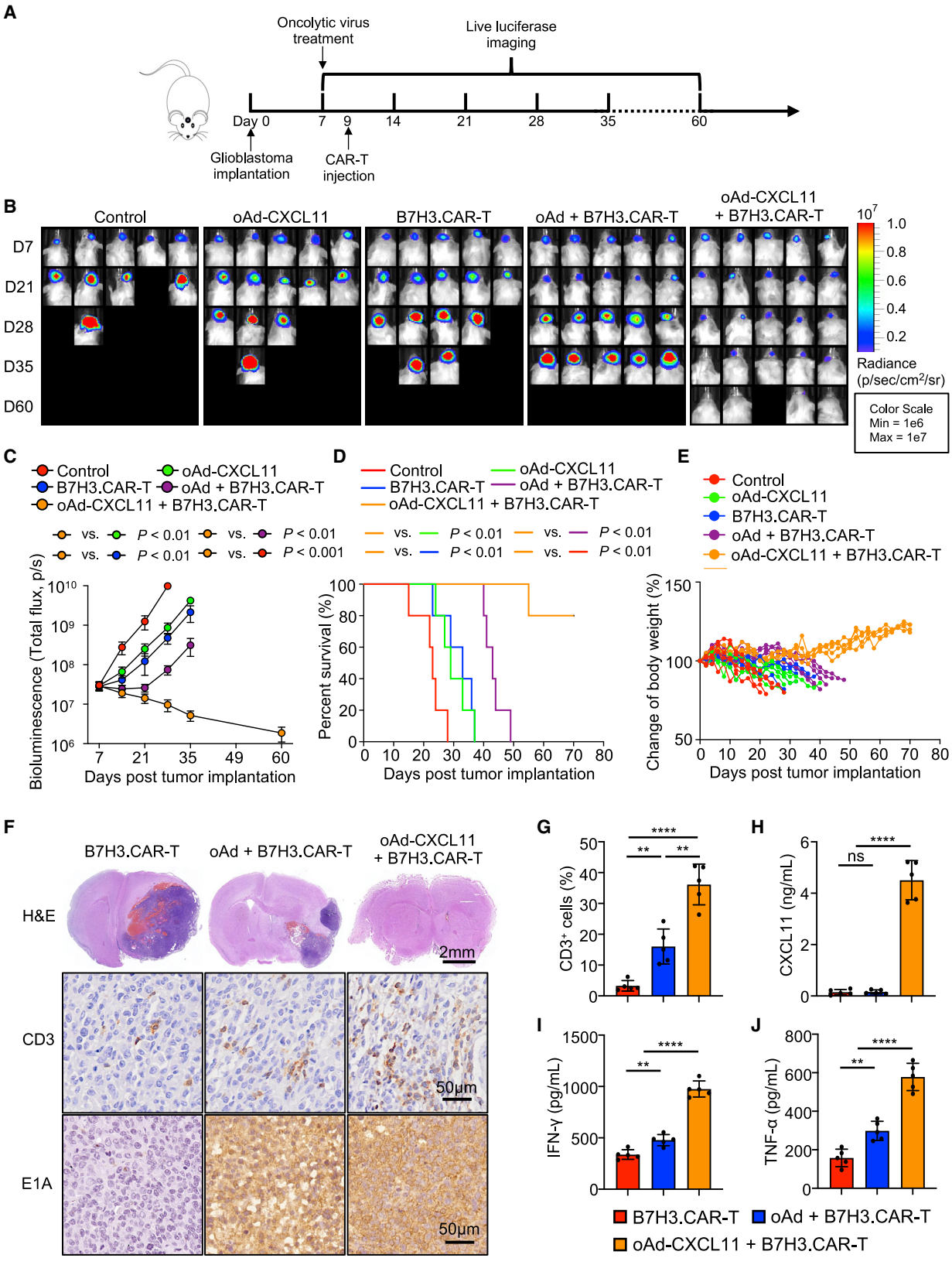

(legend on next page)

subsequently released chemokine CXCL11 to recruit CAR-T cells into the tumor sites. Nishio and colleagues genetically engineered an oncolytic adenovirus to express the chemokine CCL5 to increase the subsequent trafficking of GD2.CAR-T cells.[43] As stated earlier, activated T and NK cells highly expressed CXCR3.[37] Therefore, CXCL11 mainly attracts activated T and NK cells, but CCL5 also recruits resting immune cells.[44] In addition, there is compelling evidence for CCL5 in the progression of many cancer types,[45–47] including GBM.[48] Therefore, CXCL11 is a superior chemokine.

This genetically modified adenovirus, oAd-CXCL11, in which the expression of E1A was regulated by the promoter of human telomerase reverse transcriptase (hTERT), thus limits virus proliferation in healthy tissue. Similarly, CV706 (an oncolytic adenovirus) was designed to express E1A under the control of prostate-specific antigen (PSA) promoter, which is highly activated in prostate cancer cells.[49] The adenovirus E3 genes were deleted except for the ADP, which enhances viral spreading and apoptosis.[50,51] The CXADR is the main receptor during the process of infection for adenovirus serotype 5,[52] which is highly expressed on GBM cell lines as well as patient-derived GBM cells in our results. *In vitro* and *in vivo*, we both demonstrated that insertion of the CXCL11 gene did not impair the infection, replication, and cytotoxicity of the oncolytic adenovirus and secreted CXCL11 during the replication within GBM cells. oAd-CXCL11 was able to increase the attraction and infiltration of CAR-T cells *in vitro* as well as in a xenograft GBM model, mainly because of the released CXCL11 within the supernatant and TME, respectively. Activation of Caspase-3 in tumor cells infected by oncolytic adenoviruses has previously been observed.[53] According to our results, we supported this observation and demonstrated that oAd-CXCL11 induced GBM cells' apoptosis *in vitro*, which was further enhanced when combined with B7H3.CAR-T cells.

For the *in vivo* study, firstly, our results showed the optimum antitumor efficacy of combinatorial treatment of oAd-CXCL11 and B7H3.CAR-T in an immunodeficient GBM model. The single administration of oAd-CXCL11 or B7H3.CAR-T elicited a moderately slower GBM progression compared with that of control, but the tumor was still in progression and eventually caused the death of the mice. This unsatisfying antitumor effect of oAd-CXCL11 or B7H3.CAR-T for the xenograft GBM model might be attributed to the insufficient CAR-T cells within the tumor sites. The combinatorial treatment resulted in complete elimination of the GBM and dramatically prolonged survival of GBM-bearing NCG mice. We confirmed that marked increased expression of CXCL11 along with subsequently improved infiltration of B7H3.CAR-T cells induced a better antitumor effect. We further established a fully immunocompetent GBM mice model to analyze the antitumor effect of oAd-CXCL11 and explore the reprograming of TME after the injection of oAd-CXCL11. To secrete corresponding chemokine for recruiting murine T cells in murine GBM models, we modified oAd-CXCL11 by replacing the human CXCL11 with murine CXCL11. In contrast to the xenograft model, our data suggested that oAd-CXCL11 monotherapy elicited potent antitumor effects compared with the results in NCG mice. A possible explanation for this is that oAd-CXCL11 could attract T cells into the TME in immunocompetent mice, which is, however, impossible in immunodeficient mice. We did demonstrate that more $CD8^+$ T cells infiltrated within the tumors induced by oAd-CXCL11, due to the role of the chemokine to enhance the infiltration of activated $CD8^+$ T lymphocytes in tumors or inflammatory tissues.[42,54–58] Finally, we assessed the combinatorial treatment effect of B7H3.CAR-T and oAd-CXCL11 in an immunocompetent GBM model. Consistent with the results of immunodeficient model, the combination therapy led to a better antitumor activity. Meanwhile, oAd-CXCL11 induced more CAR-T cell infiltration into tumor sites.

In addition, TME analysis indicated that, after injection with oAd-CXCL11, higher levels of infiltrated NK cells and M1-like macrophages, as well as lower levels of infiltrated M2-like macrophages, Tregs, and MDSCs, were observed in the tumor sites. These alterations of the types of immune cells within the TME might be induced by the chemokine CXCL11, given the evidence that chemotaxis of activated T and NK cells can be increased by CXCL11. CXCL11 can increase the chemotaxis of activated T cells and NK cells,[42,59] and potentially suppress M2 macrophage polarization in a murine cancer model.[60] The presence of cytotoxic $CD8^+$ T cells, NK cells, and M1 macrophages within the TME is generally associated with regression of tumors as well as a favorable prognosis.[61–64] In contrast, infiltration of Tregs, M2 macrophages, and MDSCs promotes tumor progression and a poor prognosis.[65,66] Besides, we elucidated that $CD8^+$ T lymphocytes were essential for eliciting the antitumor effect. Therefore, the results suggested that oAd-CXCL11 had a potent antitumor effect that was mainly underpinned by oAd-CXCL11-elicited TME reprograming from a cold immunosuppressive to a hot immunosupportive state.

The oncolytic virus was administered intratumorally in our model, since it is the preferred route of infusion for oncolytic adenoviruses

Figure 5. A comparison of combined therapy and monotherapy for improving *in vivo* CAR-T therapy in a human GBM orthotopic model

(A) Experimental timeline. An orthotopic human GBM mice model was utilized by intracranial administration of 1×10^5 GBM23-Luc cells into NCG mice. On the seventh day, mice were intratumorally administered with 5×10^8 PFU of oAd, oAd-CXCL11, or vehicle control. Two days after virus administration, 5×10^6 B7H3.CAR-T cells or vehicle control were intravenously administered. (B) Representative images of GBM23-Luc growth in mice after different treatments. (C) The change of tumor total flux (p/s) in different groups. (D) Survival times of tumor-bearing mice were analyzed using the Kaplan-Meier method with the log rank test (n = 5). (E) A body weight measurement was taken once every other day for each experimental mouse. (F) H&E staining of the specimen isolated from experimental mice (scale bar, 2 mm) and immunostaining of CD3 and E1A (scale bar, 50 μm). (G) The ratio of $CD3^+$ cells per field in groups with different treatments. (H–J) Detection of CXCL11 (H), IFNγ (I), and TNFα (J) by ELISA in tumor homogenates harvested from experimental mice. The statistical analysis was estimated by one-way ANOVA with Tukey's correction. Data are presented as mean values ± SD. $^{**}p < 0.01$; $^{****}p < 0.0001$; ns, not significant.

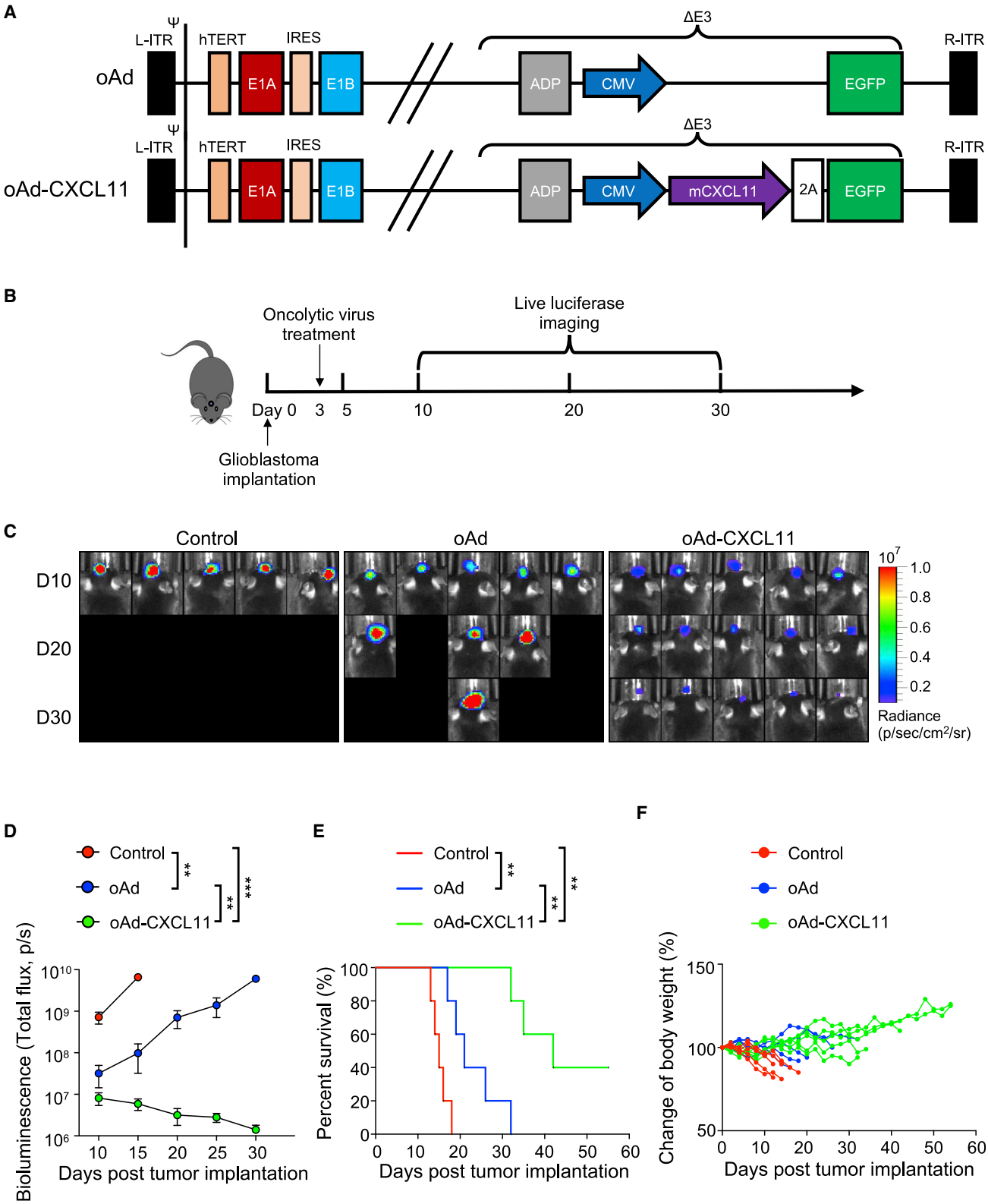

(legend on next page)

in clinical trials. However, further studies are needed to demonstrate whether this method is suitable or not for patients suffering from metastatic cancers. In the current study, our data indicated that, when oAd-CXCL11 infected tumor cells, CXCL11 was secreted during viral replication and recruited CAR-T cells into tumors, thus enhancing the tumor infiltration of CAR-T cells. In addition, this CXCL11-armed oncolytic adenovirus reprogramed immunosuppressive TME, converting a cold tumor to a hot tumor, resulting in enhanced antitumor activities.

Another promising strategy to improve the infiltration of adoptively transferred cells for solid tumors is to arm tumor-specific T cells with tumor-specific chemokine receptors. Lesch and colleagues showed that CXCR6 overexpressing improved the trafficking of adoptively transferred T cells into TME and enhanced the antitumor efficacy.[67] A recently published article screened the differentially expressed genes for chemokines between glioblastoma and normal tissue. This analysis found that seven chemokines, namely CXCL1, CXCL13, CXCL5, CCL28, CCL18, CCL8, and CCL2, were highly expressed in glioblastoma.[68] By utilizing chemotaxis of these existing chemokines in GBM, engineering T cells to express the corresponding receptor would be another way to enhance the T cell infiltration. Although further investigations are needed to verify this concept in GBM, it may be a potential therapeutic strategy to promote the antitumor efficacy of adoptive T cell therapy.

In summary, this study has shown an enhanced therapeutic response of combining oAd armed with CXCL11 and CAR-T cells by promoting the trafficking of CAR-T cells. This CXCL11-armed oncolytic adenovirus can also reprogram the immunosuppressive TME of GBM, thus inducing a potent antitumor effect and prolonged survival. Given the current clinical limitations of CAR-T cells therapy against solid cancers, the combinatorial strategy of OVs with CAR-T cells represents an exciting new cancer immunotherapy approach for future clinical study.

MATERIALS AND METHODS

Ethical approval

The experiments on animals were in performed compliance with the ethical standards of Sichuan University West China Hospital. All PBMC samples from healthy donors and GBM patients as well as tumor samples obtained from GBM patients were approved by Sichuan University West China Hospital Biomedical Ethics Committee (2018-061). All healthy donors and GBM patients provided written informed consent.

Cells

The 293A, 293T, A549, U251, A172, U87, T98G, H4, and GL261 were obtained from the ATCC. GBM23 was developed at West China Hospital. U87 cells transduced with mCherry-expression lentivirus vectors were named U87-mCherry. GBM23-Luc were isolated from a GBM patient and genetically engineered to carry the luciferase gene (Luc). All these cells were cultured in the standard protocol.

Mice

Six- to 8-week-old immunodeficient NCG female mice and immunocompetent C57BL/6 female mice were obtained from GemPharmatech. Mice were kept in pathogen-free conditions and on a typical 12 h:12 h light-dark cycle.

Oncolytic adenoviruses

All oncolytic adenoviruses were produced by a double-plasmid system, which includes a delta E1, E3 human adenovirus serotype 5 (Ad5) plasmid, pBHgloxΔE1, E3, and a shuttle vector, pDC316. The E1 region of adenovirus was regulated by the TERT tumor-specific promoter, followed by E1A-IRES-E1B genes. The ADP was incorporated into the E3 region, which means the E3 gene of adenovirus was deleted except for the ADP gene. The human or murine CXCL11 gene was then inserted into the E3 region with or without the EGFP gene, where its expression was regulated by a cytomegalovirus (CMV) promoter. All adenoviruses were packaged and propagated in the adenovirus packaging cell line, 293A. To collect the viruses, both cells and supernatants were collected 1 week after transfection of the double plasmids, then lysed through three consecutive freeze-thaw cycles and centrifuged. To amplify virus production, the lysate was transferred to more fresh plates with 293A cells. When at least half of the cells were rounded, both cells and supernatants were collected, lysed by three consecutive freeze-thaw cycles, and centrifuged at 1,500 $\times$ *g* for 5 min. By repeating the above procedure, more cell lysate was collected to further amplify the virus production. The cell lysate containing viruses was concentrated by PEG8000 and then purified by double CsCl density gradient ultracentrifugation. The virus was titrated using plaque forming assay and was stored at -80°C until ready for use.

Oncolysis and viral production experiment

The MTT kit was used to measure oncolysis *in vitro*. Briefly, cells were seeded (8,000 cells/well) for 24 h. Then different concentrations of viruses were added to the cells, and, 48 h later, cell viability was detected using MTT assay. Normalization was performed on virus-infected cells (percentage viability) against mock-infected cells. The $TCID_{50}$ assay was used to analyze the replication of the virus. Briefly, U87,

Figure 6. A comparison of oAd-CXCL11 and oAd for the antitumor efficacy in an immunocompetent mouse GBM model

(A) Schema of oncolytic adenoviruses. Top: genetic map of control oncolytic adenovirus, oAd, with deletion of E3 region sparing ADP, insertion of the hTERT promoter into the E1 region, and insertion of EGFP gene into the E3 region. Bottom: genetic map of oAd-CXCL11 showing the inserted coding gene of the murine CXCL11. (B) Experimental timeline. An immunocompetent GBM mice model was utilized by intracranial administration of 1×10^5 GL261 mouse GBM cells into C57BL/6 mice. On the third day, mice were intratumorally administered with 5×10^8 PFU of oAd, oAd-CXCL11, or vehicle control. (C) Representative images of GL261 growth in mice after different treatments. (D) The change of tumor total flux (p/s) in different groups. (E) Survival times of tumor-bearing mice were analyzed using the Kaplan-Meier method with the log rank test (n = 5). (F) A body weight measurement was taken once every other day for each experimental mouse. Data are presented as mean values ± SD. $^{**}p < 0.01$, $^{***}p < 0.001$.

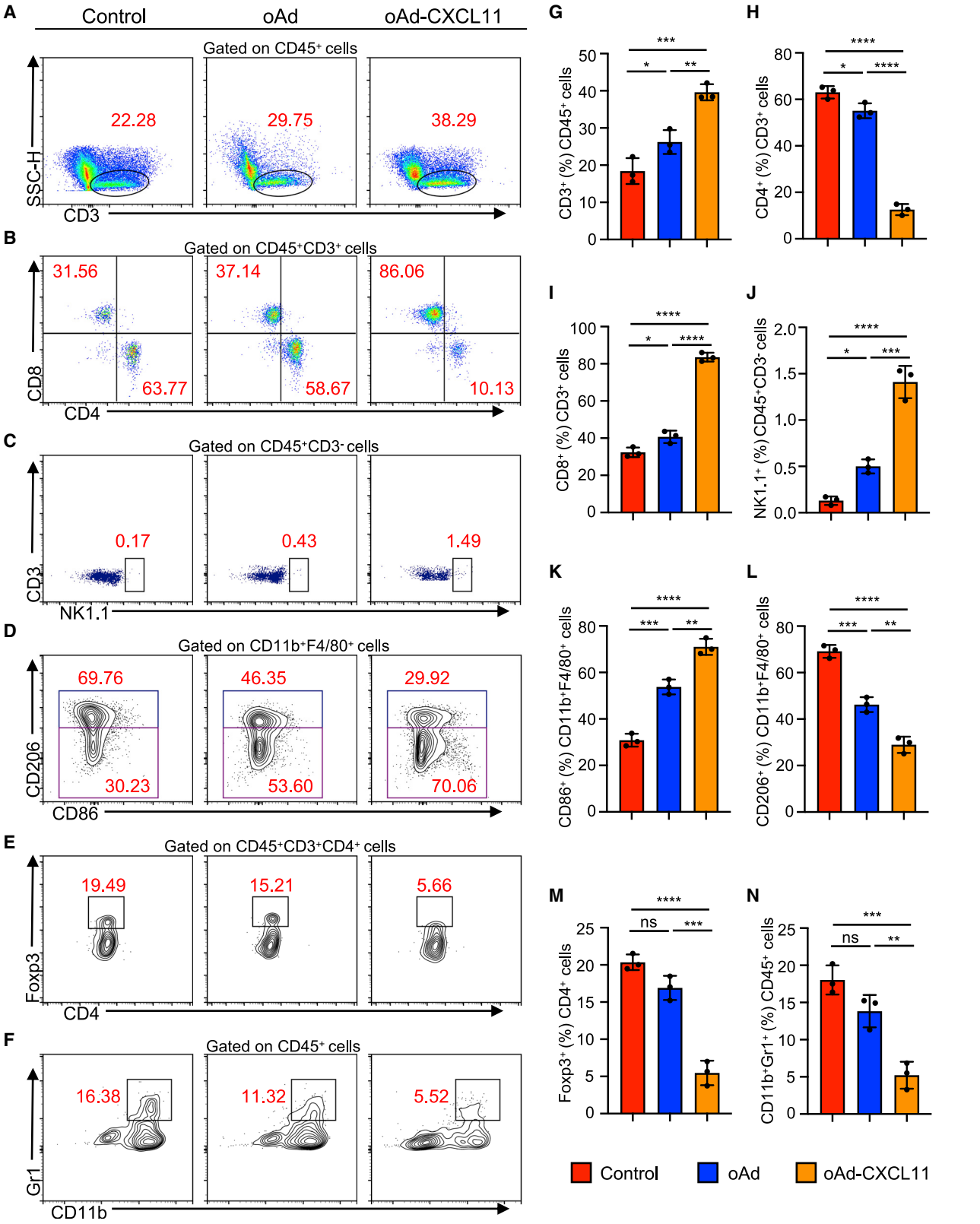

(legend on next page)

U251, and GBM23 cells were plated for 24 h and infected with oAd or oAd-CXCL11 at an MOI of 0.1 or 1. The infection medium was removed and fresh medium was added 2 h after infection. The virus titers were measured using the $TCID_{50}$ assay at various times after infection.

CAR vector construction and transduction of human and murine T cells

For human T cells, the B7H3-targeted CAR construction consisted of CD8α signal peptide, B7H3-targeted ScFv, hinge, CD8 transmembrane domain, the costimulatory domain of human 4-1BB, and CD3ζ. Based on a previously published sequence, human B7H3-targeted ScFv was synthesized (Table S1).[69] HEK-293T was cotransfected with the CAR vector and two packaging plasmids (pMD.2G and psPAX2) by using polyethyleneimine (PEI). At 48 h and 72 h post transfection, the supernatant was harvested, filtered through a 0.45-μm filter (Millipore), and then ultracentrifuged at 100,000 × *g* for 120 min at 4°C. Concentrated viruses were resuspended and stored at −80°C. Lentivirus was titrated using $TCID_{50}$ assay. For T cell isolation, PBMCs from GBM patients or healthy donors were harvested using gradient centrifugation (800 × *g*; 20 min). Collected PBMCs were cultured with 15% fetal calf serum (FCS), 100 μg/mL streptomycin, and 100 U/mL penicillin in an incubator at 37°C with 5% CO_2. T cells were stimulated with OKT3 (200 ng/mL, BioLegend), CD28.2 (120 ng/mL, BioLegend), and simultaneously supplemented with human interleukin (IL) 2 (100 U/mL) and IL-15 (1 ng/mL). After stimulating for 48 h, activated T lymphocytes were transduced with lentiviruses (MOI = 10) with RetroNectin-coated (Takara) plates (800 × Ig; 1.5 h), and simultaneously supplemented with human IL-2 and IL-15. Then, 12 h later, T cells were harvested and supplemented with IL-2 and IL-15 for about 8 days. Control T cells were produced by similar methods.

For murine T cells, the B7H3.CAR construction includes murine CD8α signal peptide, B7H3-targeted ScFv, hinge, murine CD8 transmembrane region, the costimulatory domain of murine 4-1BB, and CD3ζ, and, to detect the CAR-transduced T cells, murine CD34 was co-expressed. The 293T were cotransfected with the CAR vector and pCL-Eco plasmid (at a ratio of 4:1) by the GeneJuice (Merck Millipore). At 48 h and 72 h post transfection, the supernatant was harvested and filtered through a 0.45-μm filter (Millipore). Isolated splenocytes were activated with murine IL-7 (Peprotech) 2 pg/μL and Concanavalin A (Sigma) 2 μg/mL for 48 h, then transduced with retroviruses with RetroNectin-coated (Takara) plates (800 g; 1.5 h), and simultaneously supplemented with human IL-2 (100 U/mL). Four days after transduction, transduced cells were administered intravenously.

Crystal violet cell viability assay

The cells were seeded (5×10^4/well) with fully supplemented media and infected with oAd or oAd-CXCL11 at an MOI of 1 combined with or without B7H3.CAR-T. At 72 h post infection, the wells were washed once and fixed in 3% paraformaldehyde for 10 min. Then 0.05% crystal violet was used to stain the fixed cells for 30 min and, after washing the cells three times with PBS, images were captured.

Western blotting

Briefly, 1×10^6 U87 cells were seeded for 12 h, then infected with oncolytic adenovirus at an MOI of 10. The infection medium was removed and added with fresh medium 2 h after infection. After 24, 48, and 72 h, the cells were harvested and lysed. Total protein amounts were quantified by BCA assay (Beyotime). Equal protein amounts were loaded and transferred to polyvinylidene fluoride (PVDF). After blocking, the PVDF was incubated with anti-E1A antibody (Abcam; 1:2,000), anti-Caspase3 (CST; 1:2,000), anti-cleaved Caspase3 (CST; 1:3,000), anti-CXCL11 (Abcam; 1:1,000) and anti-β-tubulin antibody (CST; 1:2,000). Next, PVDF was incubated with HRP-conjugated secondary antibody (Beyotime; 1:2.000). Western blotting results were analyzed digitally (Clinx Science Instruments, Chemiscope 5300).

Flow cytometry

Flow cytometric assay was utilized to analyze the expression levels of CXADR, CXCR3, and B7H3. Briefly, cells were washed three times, then their Fc receptor was blocked for 30 min. Phycoerythrin (PE) Texas red channel was used to detect CAR-T cells. B7H3-targeted APC-conjugated antibody (BioLegend, 351005) was used to detect B7H3 expression in GBM cells. The following antibodies were used: CXADR (Abcam, ab275683), B7H3 (BioLegend, 351005), and CXCR3 (BioLegend, 353703). For the tumor immune microenvironment analysis, tumor tissues from mice with different treatments were collected. Single-cell suspensions were harvested using collagenase type IV (Sigma-Aldrich, C4-BIOC) and DNase-I (Roche, 10104159001). After digestion, the suspensions were filtered by a 70-μm filter (BD Falcon), blocked with CD16/CD32 antibody (BioLegend, 40477) and dead cells were stained with Zombie Violet(BioLegend, 423113). Fluorescent antibodies recognizing murine CD45-PerCP (BioLegend, 103132), CD3-APC-Cy7 (BD, 560590), CD4-FITC (BD, 553650), CD8-BV510 (BioLegend, 100752), NK1.1-APC (BioLegend, 108709), CD11b-FITC (BioLegend, 101206), F4/80-PE (BioLegend, 123110), CD86-PE-Cy7 (BD, 560582), CD206-APC (BD, 565250), Foxp3-PE (BioLegend, 126404), Gr1-BV510 (BioLegend, Cat108438), and CD34 (Thermo Fisher, 14-0341-82) were used in this assay. All flow cytometry experiments were performed using ACEA NovoCyte (Agilent Biosciences).

Figure 7. The immune microenvironment of GL261 tumors was examined using flow cytometry

Representative images of (A) T cells, (B) $CD4^+$ and $CD8^+$ T cells, (C) NK cells, (D) M1 or M2 macrophages, (E) regulatory T cells (Tregs), and (F) myeloid-derived suppressor cells (MDSCs). (G) Summary data of (A). (H and I) Summary data of (B). (J) Summary data of (C). (K and L) Summary data of (D). (M) Summary data of (E). (N) Summary data of (F). The statistical analysis was estimated by one-way ANOVA with Tukey's correction. Data are presented as mean values ± SD. *$p < 0.05$, **$p < 0.01$, ***$p < 0.001$, ****$p < 0.0001$.

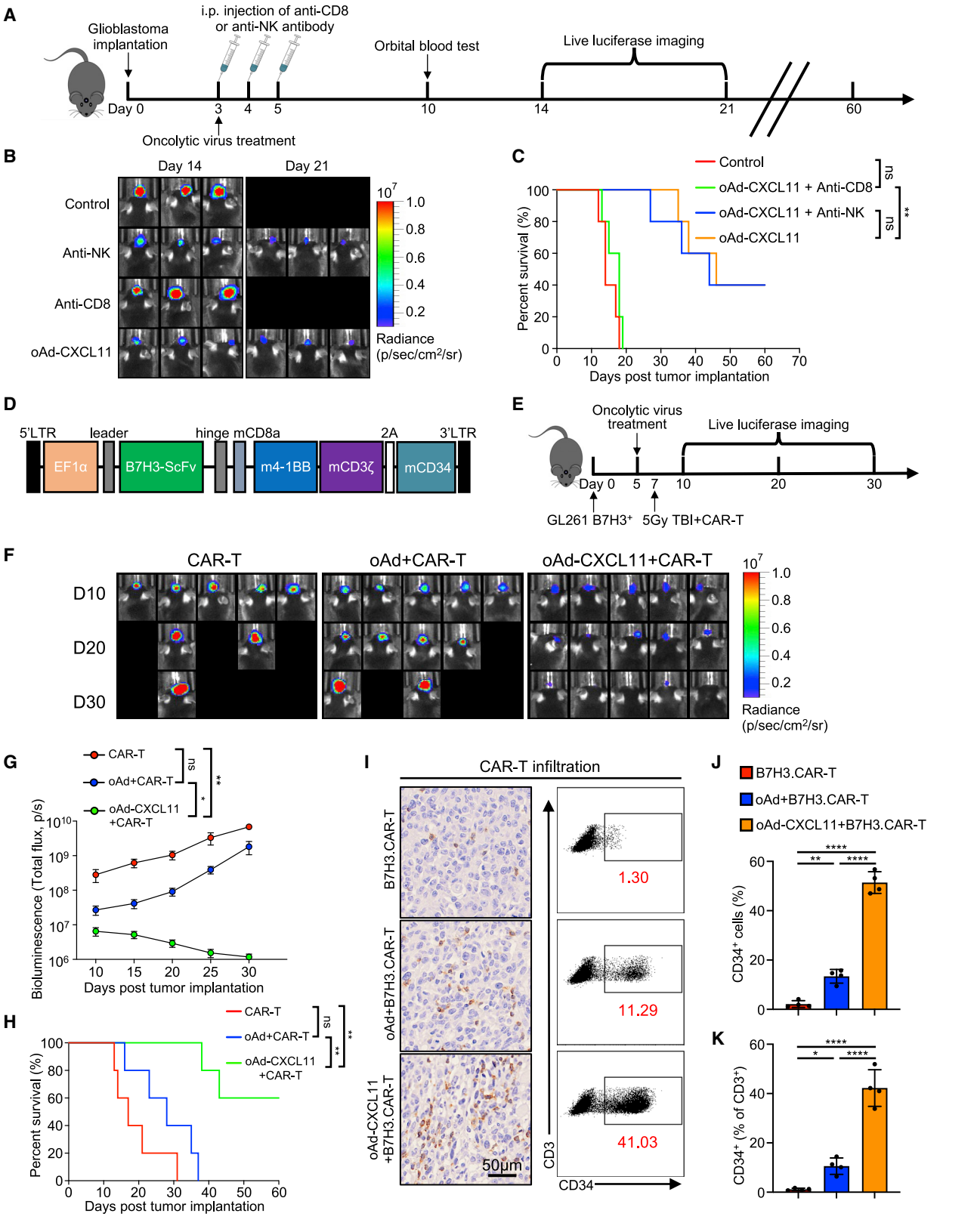

(legend on next page)

Apoptosis analysis

For apoptosis analysis, GBM cells were incubated with oncolytic adenovirus (MOI = 1). The infection medium was removed and fresh medium added 2 h after infection. After 24 h, cells were collected and stained with 7-AAD and Annexin V for 20 min, and then immediately analyzed using the NovoCyte Flow Cytometer (Agilent Biosciences). The experiments were performed in triplicate.

xCELLigence

To determine tumor cell killing, the xCELLigence RTCA (Agilent Biosciences) was used. Briefly, tumor cells were plated at 8,000 cells per well. After 24 h, cells were treated with saline control, oAd or oAd-CXCL11 (MOI = 0.01), and B7H3.CAR-T (E:T = 1:4) or vehicle control. Every 15 min, a reading was recorded and the cells were monitored for 70 h. Cell sensor impedance was defined as the cell index (CI).

3D tumor spheroids coculture assays

The 3D tumor spheroids were prepared by seeding U87 or U87-mCherry cells in ultra-low attachment plates, cultured with DMEM/F12 media (Gibco) and added to 1% B27 (Thermo Fisher Scientific), 10 pg/μL human recombinant fibroblast growth factor (FGF) (Sino Biological), and 10 pg/μL human recombinant epidermal growth factor (EGF) (Sino Biological) for a week. For the chemotaxis experiment, 3D tumor spheroids of U87-mCherry cells were infected with oAd or oAd-CXCL11 at an MOI of 1 for 24 h. Then B7H3.CAR-T cells (5×10^4) were added to the wells. Images were captured 24 h after coculture by a confocal microscope (Zeiss 880). For the cytotoxicity experiment, 3D tumor spheroids of U87 cells were infected with oAd, oAd-CXCL11, or saline control at an MOI of 1 for 24 h. Then B7H3.CAR-T cells (5×10^4) or saline control were added to the wells. 3D tumor spheroids of U87 cells were stained with Calcein/PI (Beyotime). Images were captured 24 h after coculture by a confocal microscope (Zeiss 880).

ELISA assay

For the ELISA assay, 1×10^5 tumor cells were seeded and infected with oAd or oAd-CXCL11 at an MOI of 1. The infection medium was removed and fresh medium was added 2 h after infection. The supernatants were then collected at 48 h from each group. The concentration of CXCL11 protein in the supernatants was measured by ELISA kits (R&D). A similar method was used to detect the production of TNFα as well as IFNγ in a 3D tumor spheroid cytotoxicity experiment. To detect the *in vivo* expression of chemokine (CXCL11) or cytokine (TNF-α and IFN-γ), tumor homogenates were collected from experimental NCG mice 18 days after OV injection for ELISA assay.

RNA-seq

Total RNA samples of T cells from four patients with GBM and four healthy donors were used for RNA-seq analyses by Shanghai OE Biotech. The raw data of this RNA-seq were submitted to sequence read archives (SRA) of the NCBI database (NCBI: PRJNA817671).

Chemotaxis assay

Migration was evaluated in 24-well plates with 5-μm pore size filters (Corning), and 5×10^4 tumor cells infected with OVs (oAd or oAd-CXCL11) at an MOI of 1 for 48h or media containing various recombinant chemokines with graded concentrations (0, 1, 10, 100 nM) were added to the bottom wells. T lymphocytes were isolated from PBMCs, transduced with CAR vector, and then cultured in media with IL-2 and IL-15 for 8 days. Then, CAR-T cells (2×10^5) were added to upper chambers. At 5 h after incubation, cells migrating to the lower chambers were counted to compare the difference in CAR-T cell migration.

In vivo experiment

For the immunodeficient GBM mice model, NCG mice were intracranially administered with 1×10^5 GBM23-Luc cells into the brain (1 mm anterior and 2 mm lateral to bregma at a 3-mm depth). Seven days later, mice were randomly distributed into five groups: saline control, oAd-CXCL11, B7H3.CAR-T, a combination of oAd plus intravenous injection of B7H3.CAR-T, and a combination of oAd-CXCL11 plus intravenous injection of B7H3.CAR-T. Groups with virus treatment were intracranially administered with 5×10^8 PFU oAd or oAd-CXCL11 in 3 μL of saline. Groups with CAR-T cell treatment received intravenous administration of 5×10^6 B7H3.CAR-T.

For the immunocompetent GBM mice model, C57BL/6 mice were intracranially administered with 1×10^5 GL261 cells. On the third day, mice were subsequently randomly distributed into three groups, including intracranial administration either with 5×10^8 PFU oAd or oAd-CXCL11 in 3 μL of saline as well as saline control. In an additional experiment, for eliminating the NK and $CD8^+$ T cells, on day 3, 4, and 5, mice were received a peritoneal injection with 500 mg of anti-NK1.1 or anti-CD8a.

In the combinational treatment experiment, $B7H3^+$ GL261 cells (1×10^5) were stereotactically implanted into the brain. Using a small animal radiation system, mice received TBI (5 Gy) to achieve depletion of endogenous lymphocytes before the oAd or CAR-T cell

Figure 8. The antitumor effect of oAd-CXCL11 is mediated by $CD8^+$ T cells, and combined therapy induces a better antitumor activity in GL261 tumors

(A) Experimental timeline. An immunocompetent GBM mice model was utilized by intracranial administration of 1×10^5 GL261 mouse GBM cells into C57BL/6 mice. On the third day, mice were intratumorally administered with 5×10^8 PFU of oAd-CXCL11 or vehicle control. Anti-NK or anti-CD8 antibodies were intraperitoneally administered on day 3, 4, and 5. (B) Representative images of GL261 growth in mice after different treatments. (C) Survival time of GL261 tumor-bearing mice. (D) Murine CAR construct. (E) Experimental timeline. (F) Representative images of GL261 growth in mice after different treatments. (G) The change of BLI (p/s) in different groups. (H) Survival of GL261 GBM-bearing mice. (I) CAR-T cell infiltration 7 days post infusion was confirmed by immunohistochemistry and flow cytometry for the marker gene CD34. Scale bar, 50 μm. (J) and (K) Quantification of (I). Survival times of tumor-bearing mice were analyzed using the Kaplan-Meier method with the log rank test (n = 5). The statistical analysis was estimated by one-way ANOVA with Tukey's correction. Data are presented as mean values ± SD. *$p < 0.05$; **$p < 0.01$; ****$p < 0.0001$; ns, not significant.

injection. Five days later, mice were intracranially administered either with 5×10^8 PFU oAd or oAd-CXCL11 in 3 μL of saline. Two days later, 5×10^6 B7H3.CAR-T was administered by intravenous injection.

Bioluminescent imaging

Implanted tumor cells expressing firefly luciferase were utilized to monitor tumor progression via bioluminescence imaging (BLI), using well-established standard procedures. In brief, the IVIS (Caliper Life Sciences) was utilized to image animals injected intraperitoneally with D-Luciferin, potassium salt (Beyotime). IVIS live animal BLI was performed at indicated time points to detect tumor growth.

Immunohistochemistry

Tumor samples from mice that received different treatments were fixed with paraformaldehyde, embedded in paraffin, sliced into sections, and stained. We conducted H&E staining and immunohistochemistry (staining of human T cells by anti-CD3 antibody, staining of oncolytic adenovirus by anti-E1A antibody, and staining of CAR-T cells by anti-CD34 antibody).

Statistical analysis

Statistical software Prism 8.0 (GraphPad) was used. Student's t test was utilized to compare two independent groups, and one-way ANOVA model with the correction of Tukey was utilized to compare three or more groups. Animal survival times were presented by the Kaplan-Meier method, and the p values were calculated and compared with the log rank test. Data are shown as mean ± SD. All tests were two sided. Differences associated with $p < 0.05$ were considered significant.

Data and materials availability

This paper presents all associated data with this study.

SUPPLEMENTAL INFORMATION

Supplemental information can be found online at https://doi.org/10.1016/j.ymthe.2022.08.021.

ACKNOWLEDGMENTS

This work was supported by the National Natural Science Foundation of China (82073404 and 81772693), Research Unit of Gene and Immunotherapy, Chinese Academy of Medical Sciences (no. 2019RU067), the Youth fund of National Natural Science Fund of China (82102898), CAMS Innovation Fund for Medical Science (CIFMS) (2021-I2M-5-075), and the Chengdu Science and Technology Project-Technical innovation research and development project (2021-YF05-00920-SN).

AUTHOR CONTRIBUTIONS

G.W. and Z.Z. designed and conducted the experiments and wrote the paper. G.W., Z.Z., K.Z., Z.W., N.Y., and X.T. conducted the experiments. H.L., Q.L., Z.W., B.Y., M.Z., and P.C. performed the data analysis. A.T. and L.Z. designed the experiments and supervised the research. All authors discussed the results and commented on the manuscript.

DECLARATION OF INTERESTS

G.W., A.T., and L.Z. have filed patents related to this work. The other authors declare no competing interests.

REFERENCES

1. Stupp, R., Mason, W.P., van den Bent, M.J., Weller, M., Fisher, B., Taphoorn, M.J.B., Belanger, K., Brandes, A.A., Marosi, C., Bogdahn, U., et al. (2005). Radiotherapy plus concomitant and adjuvant temozolomide for glioblastoma. N. Engl. J. Med. *352*, 987–996.
2. Tan, A.C., Ashley, D.M., López, G.Y., Malinzak, M., Friedman, H.S., and Khasraw, M. (2020). Management of glioblastoma: state of the art and future directions. CA. Cancer J. Clin. *70*, 299–312.
3. Medikonda, R., Dunn, G., Rahman, M., Fecci, P., and Lim, M. (2021). A review of glioblastoma immunotherapy. J. Neurooncol. *151*, 41–53.
4. Johnson, P.C., and Abramson, J.S. (2022). Engineered T cells: CAR T cell therapy and beyond. Curr. Oncol. Rep. *24*, 23–31.
5. Lim, W.A., and June, C.H. (2017). The principles of engineering immune cells to treat cancer. Cell *168*, 724–740.
6. Maggs, L., Cattaneo, G., Dal, A.E., Moghaddam, A.S., and Ferrone, S. (2021). CAR T cell-based immunotherapy for the treatment of glioblastoma. Front. Neurosci. *15*, 662064.
7. Sarvaiya, P.J., Guo, D., Ulasov, I., Gabikian, P., and Lesniak, M.S. (2013). Chemokines in tumor progression and metastasis. Oncotarget *4*, 2171–2185.
8. Matsumura, S., Wang, B., Kawashima, N., Braunstein, S., Badura, M., Cameron, T.O., Babb, J.S., Schneider, R.J., Formenti, S.C., Dustin, M.L., et al. (2008). Radiation-induced CXCL16 release by breast cancer cells attracts effector T cells. J. Immunol. *181*, 3099–3107.
9. Novak, L., Igoucheva, O., Cho, S., and Alexeev, V. (2007). Characterization of the CCL21-mediated melanoma-specific immune responses and in situ melanoma eradication. Mol. Cancer Ther. *6*, 1755–1764.
10. Vandercappellen, J., Van Damme, J., and Struyf, S. (2008). The role of CXC chemokines and their receptors in cancer. Cancer Lett. *267*, 226–244.
11. Zhang, Y., Guan, X.-Y., and Jiang, P. (2020). Cytokine and chemokine signals of T-cell exclusion in tumors. Front. Immunol. *11*, 594609.
12. Harlin, H., Meng, Y., Peterson, A.C., Zha, Y., Tretiakova, M., Slingluff, C., McKee, M., and Gajewski, T.F. (2009). Chemokine expression in melanoma metastases associated with CD8+ T-cell recruitment. Cancer Res. *69*, 3077–3085.
13. Andersson, A., Yang, S.-C., Huang, M., Zhu, L., Kar, U.K., Batra, R.K., Elashoff, D., Strieter, R.M., Dubinett, S.M., and Sharma, S. (2009). IL-7 promotes CXCR3 ligand-dependent T cell antitumor reactivity in lung cancer. J. Immunol. *182*, 6951–6958.
14. Mlecnik, B., Tosolini, M., Charoentong, P., Kirilovsky, A., Bindea, G., Berger, A., Camus, M., Gillard, M., Bruneval, P., Fridman, W.-H., et al. (2010). Biomolecular network reconstruction identifies T-cell homing factors associated with survival in colorectal cancer. Gastroenterology *138*, 1429–1440.
15. Li, K., Zhu, Z., Luo, J., Fang, J., Zhou, H., Hu, M., Maskey, N., and Yang, G. (2015). Impact of chemokine receptor CXCR3 on tumor-infiltrating lymphocyte recruitment associated with favorable prognosis in advanced gastric cancer. Int. J. Clin. Exp. Pathol. *8*, 14725–14732.
16. Kaufman, H.L., Kohlhapp, F.J., and Zloza, A. (2016). Oncolytic viruses: a new class of immunotherapy drugs. Nat. Rev. Drug Discov. *15*, 660.
17. Lichty, B.D., Breitbach, C.J., Stojdl, D.F., and Bell, J.C. (2014). Going viral with cancer immunotherapy. Nat. Rev. Cancer *14*, 559–567.
18. Guo, Z.S., Liu, Z., and Bartlett, D.L. (2014). Oncolytic immunotherapy: dying the right way is a key to eliciting potent antitumor immunity. Front. Oncol. *4*, 74.
19. Galluzzi, L., Buqué, A., Kepp, O., Zitvogel, L., and Kroemer, G. (2017). Immunogenic cell death in cancer and infectious disease. Nat. Rev. Immunol. *17*, 97–111.

20. Harrington, K., Freeman, D.J., Kelly, B., Harper, J., and Soria, J.-C. (2019). Optimizing oncolytic virotherapy in cancer treatment. Nat. Rev. Drug Discov. *18*, 689–706.

21. Heo, J., Reid, T., Ruo, L., Breitbach, C.J., Rose, S., Bloomston, M., Cho, M., Lim, H.Y., Chung, H.C., Kim, C.W., et al. (2013). Randomized dose-finding clinical trial of oncolytic immunotherapeutic vaccinia JX-594 in liver cancer. Nat. Med. *19*, 329–336.

22. Tomaszewski, W., Sanchez-Perez, L., Gajewski, T.F., and Sampson, J.H. (2019). Brain tumor microenvironment and host state: implications for immunotherapy. Clin. Cancer Res. *25*, 4202–4210.

23. Di Paolo, N.C., Miao, E.A., Iwakura, Y., Murali-Krishna, K., Aderem, A., Flavell, R.A., Papayannopoulou, T., and Shayakhmetov, D.M. (2009). Virus binding to a plasma membrane receptor triggers interleukin-1 alpha-mediated proinflammatory macrophage response in vivo. Immunity *31*, 110–121.

24. Prestwich, R.J., Errington, F., Diaz, R.M., Pandha, H.S., Harrington, K.J., Melcher, A.A., and Vile, R.G. (2009). The case of oncolytic viruses versus the immune system: waiting on the judgment of Solomon. Hum. Gene Ther. *20*, 1119–1132.

25. Ager, A., Watson, H.A., Wehenkel, S.C., and Mohammed, R.N. (2016). Homing to solid cancers: a vascular checkpoint in adoptive cell therapy using CAR T-cells. Biochem. Soc. Trans. *44*, 377–385.

26. Berlato, C., Khan, M.N., Schioppa, T., Thompson, R., Maniati, E., Montfort, A., Jangani, M., Canosa, M., Kulbe, H., Hagemann, U.B., et al. (2017). A CCR4 antagonist reverses the tumor-promoting microenvironment of renal cancer. J. Clin. Invest. *127*, 801–813.

27. Marshall, L.A., Marubayashi, S., Jorapur, A., Jacobson, S., Zibinsky, M., Robles, O., Hu, D.X., Jackson, J.J., Pookot, D., Sanchez, J., et al. (2020). Tumors establish resistance to immunotherapy by regulating T(reg) recruitment via CCR4. J. Immunother. Cancer *8*.

28. Zamarin, D., Hamid, O., Nayak-Kapoor, A., Sahebjam, S., Sznol, M., Collaku, A., Fox, F.E., Marshall, M.A., and Hong, D.S. (2020). Mogamulizumab in combination with durvalumab or tremelimumab in patients with advanced solid tumors: a phase I study. Clin. Cancer Res. *26*, 4531–4541.

29. Balkwill, F. (2004). The significance of cancer cell expression of the chemokine receptor CXCR4. Semin. Cancer Biol. *14*, 171–179.

30. Domanska, U.M., Kruizinga, R.C., Nagengast, W.B., Timmer-Bosscha, H., Huls, G., de Vries, E.G.E., and Walenkamp, A.M.E. (2013). A review on CXCR4/CXCL12 axis in oncology: no place to hide. Eur. J. Cancer *49*, 219–230.

31. Sacco, A., Roccaro, A.M., Ma, D., Shi, J., Mishima, Y., Moschetta, M., Chiarini, M., Munshi, N., Handin, R.I., and Ghobrial, I.M. (2016). Cancer cell dissemination and homing to the bone marrow in a zebrafish model. Cancer Res. *76*, 463–471.

32. Reif, K., Ekland, E.H., Ohl, L., Nakano, H., Lipp, M., Förster, R., and Cyster, J.G. (2002). Balanced responsiveness to chemoattractants from adjacent zones determines B-cell position. Nature *416*, 94–99.

33. Sallusto, F., Lenig, D., Förster, R., Lipp, M., and Lanzavecchia, A. (1999). Two subsets of memory T lymphocytes with distinct homing potentials and effector functions. Nature *401*, 708–712.

34. Szanya, V., Ermann, J., Taylor, C., Holness, C., and Fathman, C.G. (2002). The subpopulation of CD4+CD25+ splenocytes that delays adoptive transfer of diabetes expresses L-selectin and high levels of CCR7. J. Immunol. *169*, 2461–2465.

35. Moon, E.K., Carpenito, C., Sun, J., Wang, L.-C.S., Kapoor, V., Predina, J., Powell, D.J.J., Riley, J.L., June, C.H., and Albelda, S.M. (2011). Expression of a functional CCR2 receptor enhances tumor localization and tumor eradication by retargeted human T cells expressing a mesothelin-specific chimeric antibody receptor. Clin. Cancer Res. *17*, 4719–4730.

36. Hong, M., Puaux, A.-L., Huang, C., Loumagne, L., Tow, C., Mackay, C., Kato, M., Prévost-Blondel, A., Avril, M.-F., Nardin, A., et al. (2011). Chemotherapy induces intratumoral expression of chemokines in cutaneous melanoma, favoring T-cell infiltration and tumor control. Cancer Res. *71*, 6997–7009.

37. Qin, S., Rottman, J.B., Myers, P., Kassam, N., Weinblatt, M., Loetscher, M., Koch, A.E., Moser, B., and Mackay, C.R. (1998). The chemokine receptors CXCR3 and CCR5 mark subsets of T cells associated with certain inflammatory reactions. J. Clin. Invest. *101*, 746–754.

38. Clark-Lewis, I., Mattioli, I., Gong, J.-H., and Loetscher, P. (2003). Structure-function relationship between the human chemokine receptor CXCR3 and its ligands. J. Biol. Chem. *278*, 289–295.

39. Van Raemdonck, K., Van den Steen, P.E., Liekens, S., Van Damme, J., and Struyf, S. (2015). CXCR3 ligands in disease and therapy. Cytokine Growth Factor Rev. *26*, 311–327.

40. Vitanza, N.A., Johnson, A.J., Wilson, A.L., Brown, C., Yokoyama, J.K., Künkele, A., Chang, C.A., Rawlings-Rhea, S., Huang, W., Seidel, K., et al. (2021). Locoregional infusion of HER2-specific CAR T cells in children and young adults with recurrent or refractory CNS tumors: an interim analysis. Nat. Med. *27*, 1544–1552.

41. Moon, E.K., Wang, L.-C., Dolfi, D.V., Wilson, C.B., Ranganathan, R., Sun, J., Kapoor, V., Scholler, J., Puré, E., Milone, M.C., et al. (2014). Multifactorial T-cell hypofunction that is reversible can limit the efficacy of chimeric antigen receptor-transduced human T cells in solid tumors. Clin. Cancer Res. *20*, 4262–4273.

42. Cole, K.E., Strick, C.A., Paradis, T.J., Ogborne, K.T., Loetscher, M., Gladue, R.P., Lin, W., Boyd, J.G., Moser, B., Wood, D.E., et al. (1998). Interferon-inducible T cell alpha chemoattractant (I-TAC): a novel non-ELR CXC chemokine with potent activity on activated T cells through selective high affinity binding to CXCR3. J. Exp. Med. *187*, 2009–2021.

43. Nishio, N., Diaconu, I., Liu, H., Cerullo, V., Caruana, I., Hoyos, V., Bouchier-Hayes, L., Savoldo, B., and Dotti, G. (2014). Armed oncolytic virus enhances immune functions of chimeric antigen receptor-modified T cells in solid tumors. Cancer Res. *74*, 5195–5205.

44. Araujo, J.M., Gomez, A.C., Aguilar, A., Salgado, R., Balko, J.M., Bravo, L., Doimi, F., Bretel, D., Morante, Z., Flores, C., et al. (2018). Effect of CCL5 expression in the recruitment of immune cells in triple negative breast cancer. Sci. Rep. *8*, 4899.

45. Aldinucci, D., and Casagrande, N. (2018). Inhibition of the CCL5/CCR5 Axis against the progression of gastric cancer. Int. J. Mol. Sci. *19*.

46. Pervaiz, A., Zepp, M., Mahmood, S., Ali, D.M., Berger, M.R., and Adwan, H. (2019). CCR5 blockage by maraviroc: a potential therapeutic option for metastatic breast cancer. Cell. Oncol. (Dordr) *42*, 93–106.

47. Singh, S.K., Mishra, M.K., Eltoum, I.-E.A., Bae, S., Lillard, J.W.J., and Singh, R. (2018). CCR5/CCL5 axis interaction promotes migratory and invasiveness of pancreatic cancer cells. Sci. Rep. *8*, 1323.

48. Kranjc, M.K., Novak, M., Pestell, R.G., and Lah, T.T. (2019). Cytokine CCL5 and receptor CCR5 axis in glioblastoma multiforme. Radiol. Oncol. *53*, 397–406.

49. DeWeese, T.L., van der Poel, H., Li, S., Mikhak, B., Drew, R., Goemann, M., Hamper, U., DeJong, R., Detorie, N., Rodriguez, R., et al. (2001). A phase I trial of CV706, a replication-competent, PSA selective oncolytic adenovirus, for the treatment of locally recurrent prostate cancer following radiation therapy. Cancer Res. *61*, 7464–7472.

50. Doronin, K., Toth, K., Kuppuswamy, M., Krajcsi, P., Tollefson, A.E., and Wold, W.S.M. (2003). Overexpression of the ADP (E3-11.6K) protein increases cell lysis and spread of adenovirus. Virology *305*, 378–387.

51. Doronin, K., Toth, K., Kuppuswamy, M., Ward, P., Tollefson, A.E., and Wold, W.S. (2000). Tumor-specific, replication-competent adenovirus vectors overexpressing the adenovirus death protein. J. Virol. *74*, 6147–6155.

52. Greber, U.F., and Flatt, J.W. (2019). Adenovirus entry: from infection to immunity. Annu. Rev. Virol. *6*, 177–197.

53. Diaconu, I., Cerullo, V., Hirvinen, M.L.M., Escutenaire, S., Ugolini, M., Pesonen, S.K., Bramante, S., Parviainen, S., Kanerva, A., Loskog, A.S.I., et al. (2012). Immune response is an important aspect of the antitumor effect produced by a CD40L-encoding oncolytic adenovirus. Cancer Res. *72*, 2327–2338.

54. Bromley, S.K., Mempel, T.R., and Luster, A.D. (2008). Orchestrating the orchestrators: chemokines in control of T cell traffic. Nat. Immunol. *9*, 970–980.

55. Hensbergen, P.J., Wijnands, P.G.J.T.B., Schreurs, M.W.J., Scheper, R.J., Willemze, R., and Tensen, C.P. (2005). The CXCR3 targeting chemokine CXCL11 has potent antitumor activity in vivo involving attraction of CD8+ T lymphocytes but not inhibition of angiogenesis. J. Immunother. *28*, 343–351.

56. Hamilton, N.H.R., Mahalingam, S., Banyer, J.L., Ramshaw, I.A., and Thomson, S.A. (2004). A recombinant vaccinia virus encoding the interferon-inducible T-cell alpha chemoattractant is attenuated in vivo. Scand. J. Immunol. *59*, 246–254.

57. Berencsi, K., Meropol, N.J., Hoffman, J.P., Sigurdson, E., Giles, L., Rani, P., Somasundaram, R., Zhang, T., Kalabis, J., Caputo, L., et al. (2007). Colon carcinoma cells induce CXCL11-dependent migration of CXCR3-expressing cytotoxic T lymphocytes in organotypic culture. Cancer Immunol. Immunother. *56*, 359–370.

58. Wendel, M., Galani, I.E., Suri-Payer, E., and Cerwenka, A. (2008). Natural killer cell accumulation in tumors is dependent on IFN-gamma and CXCR3 ligands. Cancer Res. *68*, 8437–8445.

59. Farber, J.M. (1997). Mig and IP-10: CXC chemokines that target lymphocytes. J. Leukoc. Biol. *61*, 246–257.

60. Oghumu, S., Varikuti, S., Terrazas, C., Kotov, D., Nasser, M.W., Powell, C.A., Ganju, R.K., and Satoskar, A.R. (2014). CXCR3 deficiency enhances tumor progression by promoting macrophage M2 polarization in a murine breast cancer model. Immunology *143*, 109–119.

61. Sato, E., Olson, S.H., Ahn, J., Bundy, B., Nishikawa, H., Qian, F., Jungbluth, A.A., Frosina, D., Gnjatic, S., Ambrosone, C., et al. (2005). Intraepithelial CD8+ tumor-infiltrating lymphocytes and a high CD8+/regulatory T cell ratio are associated with favorable prognosis in ovarian cancer. Proc. Natl. Acad. Sci. USA *102*, 18538–18543.

62. Ménard, S., Tomasic, G., Casalini, P., Balsari, A., Pilotti, S., Cascinelli, N., Salvadori, B., Colnaghi, M.I., and Rilke, F. (1997). Lymphoid infiltration as a prognostic variable for early-onset breast carcinomas. Clin. Cancer Res. *3*, 817–819.

63. Grabowski, M.M., Sankey, E.W., Ryan, K.J., Chongsathidkiet, P., Lorrey, S.J., Wilkinson, D.S., and Fecci, P.E. (2021). Immune suppression in gliomas. J. Neurooncol. *151*, 3–12.

64. Sica, A., and Mantovani, A. (2012). Macrophage plasticity and polarization: in vivo veritas. J. Clin. Invest. *122*, 787–795.

65. Galdiero, M.R., Garlanda, C., Jaillon, S., Marone, G., and Mantovani, A. (2013). Tumor associated macrophages and neutrophils in tumor progression. J. Cell. Physiol. *228*, 1404–1412.

66. De Leo, A., Ugolini, A., and Veglia, F. (2020). Myeloid cells in glioblastoma microenvironment. Cells *10*.

67. Lesch, S., Blumenberg, V., Stoiber, S., Gottschlich, A., Ogonek, J., Cadilha, B.L., Dantes, Z., Rataj, F., Dorman, K., Lutz, J., et al. (2021). T cells armed with C-X-C chemokine receptor type 6 enhance adoptive cell therapy for pancreatic tumours. Nat. Biomed. Eng. *5*, 1246–1260.

68. Gao, W., Li, Y., Zhang, T., Lu, J., Pan, J., Qi, Q., Dong, S., Chen, X., Su, Z., and Li, J. (2022). Systematic analysis of chemokines reveals CCL18 is a prognostic biomarker in glioblastoma. J. Inflamm. Res. *15*, 2731–2743.

69. Ahmed, M., Cheng, M., Zhao, Q., Goldgur, Y., Cheal, S.M., Guo, H., Larson, S.M., and Cheung, N.V. (2015). Humanized affinity-matured monoclonal antibody 8H9 has potent antitumor activity and binds to FG loop of tumor antigen B7-H3. J. Biol. Chem. *290*, 30018–30029.